RSC Advances

PAPER

View Article Online
View Journal | View Issue

Check for updates

Cite this: *RSC Adv.*, 2025, **15**, 44691

Catalytic co-pyrolysis of waste pistachio nutshells and polystyrene: optimisation of parameters, and catalyst loading on the products yield and composition

Harsh Desai,[a] Rohit Dutta,[a] Tanushka Florence Panicker,[a] Sampath Chinnam,[b] Ranjeet Kumar Mishra,*[a] Srinivas Kini Manjeshwar[a] and Pradeep Kumar[c]

The increasing energy demand and environmental challenges associated with fossil fuel use have spurred interest in renewable energy sources, particularly biofuels derived from waste biomass and plastics. This study investigates the catalytic co-pyrolysis of pistachio nutshells (PNS) and polystyrene (PS) to produce pyrolysis oil and char with enhanced fuel properties. The experiments were conducted in a semi-batch reactor under varying temperatures (500–650 °C), 30 °C min^{-1} heating rate, and 100 mL min^{-1} inert gas flow rate. Furthermore, PS loadings (20–50 wt%) and CuO loadings (5 and 10 wt%) were employed to improve the pyrolysis oil characteristics. The optimum conditions were found to be 550 °C with 30 wt% PS and 5 wt% CuO loading, yielding a maximum bio-oil output of 49 wt%. The characterisation of the pyrolysis oil revealed significant improvements in fuel quality with catalytic treatment, including an increased higher heating value (HHV) of 35.90 MJ kg^{-1}, reduced oxygen content (11.69 wt%), and lower viscosity (36.40 cP). Similarly, the resulting biochar exhibited high carbon content (76.57 wt%), low ash and moisture content (<1%), and enhanced calorific value, indicating its potential as a solid fuel or soil amendment. FTIR and NMR analyses confirmed the reduction of oxygenated functional groups and the presence of desirable hydrocarbon structures in the oil, while XRD and SEM analyses demonstrated improved structural properties of the char. The results highlight the synergistic benefits of co-processing biomass and plastic waste, as well as the catalytic role of CuO in enhancing product quality. This approach offers a sustainable waste-to-energy pathway, promoting circular economy principles and advancing the production of renewable fuels from mixed solid wastes.

Received 18th August 2025
Accepted 11th November 2025

DOI: 10.1039/d5ra06092c

rsc.li/rsc-advances

Open Access Article. Published on 17 November 2025. Downloaded on 2/17/2026 10:41:37 PM.
This article is licensed under a Creative Commons Attribution-NonCommercial 3.0 Unported Licence.

1. Introduction

The rising global energy demand, depletion of fossil fuel reserves, and escalating environmental concerns have underscored the urgent need for sustainable and renewable energy alternatives.[1] Among various options, biofuels derived from biomass have garnered significant attention due to their carbon-neutral nature and potential to valorise waste materials.[2] According to estimates, the agriculture sector alone produces 140 billion tonnes of biomass waste annually, demonstrating the great potential for the utilisation of biomass.[3] Just 40% of this is used to generate power, fuel, and feed.[3] A serious concern for the ecology and climate is the incineration of most biomass residues.[4] However, of the 181.5 billion tonnes of lignocellulosic biomass, the most prevalent kind of biomass that is created each year from agriculture and forestry waste, only 8.20 billion tonnes are used.[4] Recycling this rich resource into biofuels is preferable to landfilling, open dumping, or incinerating the remaining underutilised biomass to potentially meet or supplement the world's renewable energy demands.[4] Reducing the use of fossil fuels, promoting zero waste of biomass, and managing biomass resource cycles are all aided by the conversion of lignocellulosic and agricultural biomass into valuable products (such as fertiliser, bioplastics, and biofuels).[3]

Plastic is utilised extensively around the world because of its affordability, adaptability, and usefulness.[5] Plastic has permeated every aspect of contemporary life, making its complete eradication all but impossible. Global industrialisation and population growth have resulted in a sharp rise in demand for consumer goods, food, energy, and technology. The amount of garbage generated worldwide has increased dramatically as a result, accounting for 44% of food waste, green waste, and

[a]*Department of Chemical Engineering, Manipal Institute of Technology, Manipal Academy of Higher Education, Manipal, Karnataka-576104, India. E-mail: ranjeet.mishra@manipal.edu*

[b]*Department of Chemistry, M. S. Ramaiah Institute of Technology, Bangalore 560 054, Karnataka, India*

[c]*Department of Chemical Engineering & Technology, Indian Institute of Technology (BHU), Varanasi 221005, Uttar Pradesh, India*

© 2025 The Author(s). Published by the Royal Society of Chemistry

Open Access Article. Published on 17 November 2025. Downloaded on 2/17/2026 10:41:37 PM. This article is licensed under a Creative Commons Attribution-NonCommercial 3.0 Unported Licence.

12% of plastic waste.[3] The amount of plastic produced annually has grown from 2 million tonnes in 1950 to 381 million tonnes in 2018, resulting in 464 million tonnes of plastic garbage annually.[6] Around 20% of plastic garbage was recycled globally, 25% was burned, and the remaining 55% was dumped in landfills or dumpsites.[6] The plastic garbage, recycling and reuse will always be preferable to landfilling or burning. However, technological obstacles (such as chemical reactions between plastic waste and the processing chemicals) and physical obstacles (such as buildup, segregation, and pretreatment to remove pollutants, colourants, or adhesives) limit the recycling of plastic trash. Using thermochemical processes to transform severely polluted and non-reformable plastics (thermosets) into fuels or energy is a good alternative.[7] Like this, turning biomass waste into biofuels will increase the global supply of renewable energy because it is produced in vast quantities each year, but it is not used to its full potential. The pyrolysis still has some advantages over the others, such as using less energy, emitting comparatively fewer harmful gases, being easier to scale up, and having portable reactors (mobile reactors).[3,8] Combining plastic waste with biomass as feedstocks for the co-pyrolysis process has grown in popularity. Biomass and plastics can be converted into char, oil, and gas *via* a variety of thermochemical processes, including pyrolysis, gasification, torrefaction, combustion, hydrothermal liquefaction, and hydrothermal carbonisation. Benefits of co-pyrolysing plastics and biomass include increased production of pyrolysis oil and char, decreased moisture content, oxygen content, viscosity, corrosivity, less hydrogen demand during upgrading, and effective resource recycling.[9]

The thermochemical process is converting feed waste into fuels and chemicals.[10] These techniques make plastics a useful resource in a circular economy. Over the past 20 years, the circular economy concept has drawn attention worldwide because it creates frameworks to close material resource loops, lessen dependency on petrochemicals, minimise imports of natural resources, reduce anthropogenic environmental effects, and mitigate climate change. Pistachio nutshells (PNS) biomass is produced in India's extensive agro-industrial sector, which is mainly unused. At the same time, the increasing amount of plastic waste poses a threat to the environment, as polystyrene (PS) is resistant to natural decomposition. In 2022, world production of pistachios was 1 million tonnes, with the United States, Iran, and Turkey combined accounting for 88% of the total. The thermochemical conversion method for turning biomass and plastic waste into useful products like char, gas, and bio-oil is pyrolysis. The liquid product obtained from the pyrolysis of biomass and plastics has two main phases: aqueous (15–30%) and organic phases (35–75%).[11] Further, the pyrolysis oil obtained from thermal pyrolysis has many drawbacks, such as high oxygen content (typically 35–50%), high water content (15–30%), highly viscous (40–100 cP), acids *etc.* Further, the presence of fine solid particles and char can cause fouling and abrasion in engine systems unless adequately filtered. The thermal pyrolysis oil has a pungent odour and contains volatile organic compounds (VOCs), making it unpleasant and potentially hazardous to handle. Therefore, upgrading this complex mixture into usable fuel typically requires energy-intensive and expensive catalytic processes and hydrotreatment under high pressure with hydrogen.

Ma *et al.* (2020) investigated catalytic pyrolysis of *Ulva prolifera* using ZSM-5, Y-Zeolite, and Mordenite. Zeolite catalysts improved pyrolysis oil by enhancing deoxygenation, increasing hydrocarbons, and reducing acidity and viscosity. They also shifted product distribution toward higher liquid yields and fewer oxygenated compounds.[12] Buyang *et al.* (2023) studied the catalytic pyrolysis of non-edible *Reutealis trisperma* oil (RTO) using raw dolomite for bio-oil production, and they reported that the use of a catalyst decreased the viscosity (3.12 cSt) and increased calorific value (41.61 MJ kg^{-1}) and density (0.85 g cm^{-3}).[13] Chireshe *et al.* (2019) conducted catalytic pyrolysis of forest residues in a kg-scale rotary kiln reactor. They reported an enhanced catalyst volatile interaction improved deoxygenation, producing an organic-rich oil with 12.60 wt% oxygen and a Higher Heating Value of 35.50 MJ kg^{-1}.[14] Table S1 lists many studies on the production of pyrolysis oil with and without a catalyst. Although the pyrolysis of plastics and biomass separately has been thoroughly studied, co-pyrolysis provides synergistic effects that can improve the production and quality of the final product.[15] Nevertheless, limited studies are available on the catalytic co-pyrolysis of feedstock combinations, like PS and PNS. The current study addresses this gap by exploring the synergistic effects of PNS and PS co-processing and assessing the catalytic influence of CuO on product yield and composition. Unlike previous studies that focused on zeolite catalysts, this study uniquely integrates waste biomass and non-recyclable plastic under catalytic conditions, optimising operational parameters to enhance liquid fuel quality. Furthermore, the novelty lies in demonstrating the role of CuO, which enhances deoxygenation, increases hydrocarbon content, reduces undesirable oxygenated compounds in pyrolysis oil, and improves the properties of the resulting char. This dual valorisation of pyrolysis oil and biochar from waste underlines a sustainable and circular waste-to-energy strategy, advancing the field of catalytic thermochemical conversion.

In light of the aforementioned research gap, the present study focuses on the thermal and catalytic co-pyrolysis of waste biomass (PNS) and plastic (PS) to produce liquid fuel. The pyrolysis experiment was performed in a semi-batch stainless steel reactor at 550 °C, 30 °C min^{-1} heating rate and 100 mL min^{-1} nitrogen gas flow rate. Further, the pyrolysis oil was characterised using ultimate analysis, heating value, FTIR, GC-MS, and ^{1}H NMR. The solid residue obtained under optimised conditions was also characterised in terms of its physical and chemical properties.

2. Materials and methods

2.1. Sample collection and preparations

Pistachio nutshell (PNS) and polystyrene (PS) were selected to produce bio-oil using pyrolysis. The pista nutshell was collected from a local industry near Manipal, whereas PS was collected from the waste dumping site at MIT Manipal. PNS was sun-dried for over a week and placed in the oven at 105 °C for 3 h.

© 2025 The Author(s). Published by the Royal Society of Chemistry

Open Access Article. Published on 17 November 2025. Downloaded on 2/17/2026 10:41:37 PM. This article is licensed under a Creative Commons Attribution-NonCommercial 3.0 Unported Licence.

PS was washed with water and sun-dried over 2–3 days, then placed in a hot air oven at 105 °C for 8 hours. Further, PNS and PS were pulverised in a grinder to get the desired particle size (<1 mm). Finally, the grounded biomass and plastic were placed in an airtight bag to prevent humidity.

2.2. Catalyst

Copper oxide (CuO, particle size: <50 nm, powder) was used for catalytic pyrolysis without any treatment. CuO was loaded at 5 and 10 wt% physically to evaluate the effect of the catalysts on liquid yield and the properties of the fuel.

2.3. Characterisation of feedstock

Proximate analysis serves as the initial step in characterising feed materials, providing key parameters such as moisture content (MC), volatile matter (VM), ash content (A), and fixed carbon (FC). The moisture and ash content were determined in accordance with ASTM D 2974-08, while volatile matter was measured according to ASTM D 4559-99. Furthermore, the ultimate analysis was performed using a CHNS/O elemental analyser (Variael Dice, Germany). Further, several factors, including size, shape, density, moisture content, surface characteristics, and compactness, influence feed bulk density (BD). Bulk density plays a crucial role in transportation and storage. BD was measured using a digital scale and a graduated cylinder, with the weight of the sample determined *via* a computerised weighing scale and its volume calculated using the graduated cylinder. The higher heating value (HHV) of the sample was determined by combusting the solid fuel in a controlled environment using an oxygen-bomb calorimeter (Parr 1108P). Lastly, the biochemical composition of the biomass was assessed using the Van Soest method.[16]

2.4. Fourier transform infrared (FTIR) analysis

Fourier transform infrared spectroscopy was utilised to classify functional groups on biomass and plastic material in samples of different ratios. A small amount of sample was mixed with oven-dried potassium bromide (KBr) powder in a 1 : 100 ratio and loaded into a sample holder. The sample was scanned at a rate of 40 scans per second with a step size of 4 cm^{-1} within the range of 400–4000 cm^{-1} wavenumbers.

2.5. Thermal analysis

Thermogravimetric analysis (TGA) was performed in a thermogravimetric analyser (TGA, STA449, NETZSCH) to assess the thermal behaviour of the sample. A sample weighing 8.0 mg was placed in an aluminum crucible and heated from 30 to 900 °C at 10 °C min^{-1} under a continuous nitrogen gas flow of 50 mL min^{-1}. The weight loss of the biomass as a function of temperature was recorded, and the data obtained were analysed using Origin software.

2.6. Experimental setup

Pistachio nutshell and polystyrene were pyrolysed in an inert environment in a cylindrical semi-batch reactor. The reactor was constructed using high-grade stainless steel (SS-304) with an internal diameter of 15 cm, an outer diameter of 16.20 cm, and a length of 50 cm. The outer surface of the furnace was also made of high-grade stainless steel, while the internal surface was lined with ceramic bricks to minimise heat loss. It was assumed that the heating was uniform throughout the reactor, ensuring negligible heat loss. The experimental setup consists of a stainless-steel reactor, a furnace, a nitrogen cylinder, a gas rotameter, a PID controller, a condenser, a thermocouple, and a liquid collection tank. A desired amount of sample (250 g per test) was loaded into the reactor and positioned vertically inside the furnace. The pyrolysis process was carried out at a specific temperature with a heating rate of 30 °C min^{-1}, while the feed particles were maintained at approximately 1 mm in diameter. The holding time was maintained at 45 minutes, allowing sufficient time to achieve equilibrium. Temperature and heating rate were regulated *via* a control panel directly connected to the furnace. The nitrogen was inserted into the reactor from the bottom section, while the top section was connected to a condenser. The nitrogen flow rate was precisely controlled using a gas rotameter and maintained at a steady rate of 100 mL min^{-1} throughout the experiment. The hot volatiles generated during pyrolysis were captured in the condenser, where condensable gases formed pyrolysis oil while non-condensable gases exited the system. After the experiment, the reactor was cooled to room temperature (25–30 °C), and the resulting biochar was collected and stored in an airtight glass jar for further analysis. The complete experimental setup for the pyrolysis process is illustrated in Fig. 1. Additionally, the yields of solid, liquid, and gaseous products were determined using eqn (1)–(3).

$$\text{Pyrolysis oil yield (wt\%)} = \frac{\text{weight of oil obtained}}{\text{weight of total feed}} \times 100 \quad (1)$$

$$\text{Char yield (wt\%)} = \frac{\text{weight of char obtained}}{\text{weight of total feed}} \times 100 \quad (2)$$

$$\text{Syngas yield (wt\%)} = 100 - [\text{pyrolysis oil yield (wt\%)} + \text{char yield (wt\%)}] \quad (3)$$

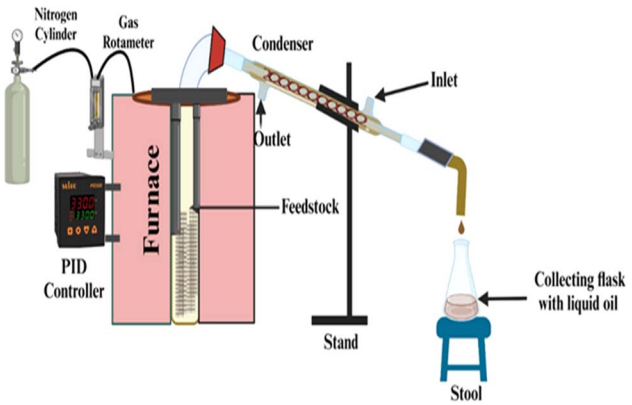

Fig. 1 Schematic representation of experimental setup.

Open Access Article. Published on 17 November 2025. Downloaded on 2/17/2026 10:41:37 PM. This article is licensed under a Creative Commons Attribution-NonCommercial 3.0 Unported Licence.

2.7. Optimization of pyrolysis process parameters

The optimisation of pyrolysis temperature, plastic loading, and catalyst concentration plays a crucial role in enhancing the yield and composition of pyrolysis oil. In this study, pyrolysis was conducted at varying temperatures (500, 550, 600 and 650 °C) to determine the optimal conditions for maximising liquid fuel production. Plastic waste was incorporated at 20, 30, and 50 wt% to assess its influence on product distribution and synergistic effects during co-pyrolysis. Higher plastic content typically enhances hydrocarbon formation but may also lead to excessive wax formation at elevated temperatures. Plastic loading at 50 wt% choked due to the formation of excess wax; thus, only 30 wt% was considered the optimum loading. Additionally, CuO catalyst was introduced at 5 and 10 wt% to facilitate catalytic cracking and improve bio-oil quality by reducing oxygenated compounds. The catalyst promotes deoxygenation, enhancing the production of valuable hydrocarbons while minimising char and gas formation. A systematic evaluation of these parameters helps identify the ideal pyrolysis conditions that balance pyrolysis oil yield, composition, and stability. The insights gained from this optimisation can contribute to the efficient valorization of biomass-plastic mixtures, offering a sustainable pathway for converting waste into high-value liquid fuels through catalytic pyrolysis.

2.8. Physicochemical characterisation of pyrolysis oil

A feasibility study of pyrolysis oil is crucial before its industrial application. Therefore, the viscosity was evaluated using a rheometer (Cone and Plate, HAKKE Rheostress 1) at 40 °C with a rotation speed of 50 rpm. The higher heating value (HHV) and elemental composition of pyrolysis oil were analysed following the procedure outlined in Section 2.3. The acidity was measured using an Eutech Waterproof pH Spear meter, while its density was determined using a density meter (Anton Paar, DMA4500M). The moisture content was assessed using a Karl Fischer water analyser (Metrohm 787 KF Titrino), and the ash content was quantified with a thermogravimetric analyser (TGA) in accordance with ASTM D5142 standards. The compositional analysis of pyrolysis oil was performed using a PerkinElmer (Clarus 600/680) gas chromatography-mass spectrometry (GC-MS) system. The GC-MS was equipped with an Elite 5 MS column (30 mm × 0.250 μm), and helium was used as the carrier gas at a constant flow rate of 0.6 mL min^{-1}. The GC program was set with an initial oven temperature of 40 °C, held for 4 min, then increased at a rate of 5 °C min^{-1} until reaching 300 °C, where it was maintained for 10 minutes. The injector temperature was set at 250 °C. Before analysis, the bio-oil was diluted with dichloromethane, filtered, and a 1 μL sample was injected into the GC system. The obtained GC-MS chromatogram was compared with the National Institute of Standards and Technology (NIST) library to identify and confirm the primary compounds and their composition. The ^1H NMR of pyrolysis oil was performed using a Bruker Ascend 400 MHz. The sample was prepared by mixing $DMSO_4$ solvent. The experiment was repeated twice, and the best results were listed in the manuscript.

2.9. Physicochemical characterisation of biochar

The proximate and elemental analyses, heating value (HHV), pH, and bulk density were determined following the methods outlined in Section 2.3. The Brunauer–Emmett–Teller (BET) surface area was measured using a BET surface area analyzer (Autosorb-iQ, Quantachrome Instruments) with ASiQwin 5 software. Prior to analysis, dried mixed wood sawdust biochar (MWSB) was degassed at 200 °C for 3 h to eliminate pore moisture. The BET analysis was conducted according to ASTM standard D6556-19 using a multi-point method, where the degassed sample underwent an adsorption/desorption process. Additionally, the water holding capacity (WHC) was assessed using a ceramic Büchner funnel, Fisher brand P8 filter paper, and deionised water. Surface morphology was examined using a field emission scanning electron microscope (FE-SEM) equipped with energy-dispersive spectroscopy (EDS). A small amount of moisture-free biochar was placed on a carbon tape-coated SEM tab, which served as the background. Imaging was performed at an accelerating voltage of 15 kV, with the biochar sample remaining uncoated.

2.10. Results analysis and data presentation

All experiments were performed in triplicate to ensure reproducibility and strengthen the reliability of the findings. The results are presented as mean ± standard deviation based on averaged measurements. A 95% confidence level was applied to assess the statistical significance of the outcomes. Furthermore, the data were visualised using suitably scaled graphs and tables to provide a clear depiction of variability and comparative trends among the samples.

3. Results and discussions

3.1. Physicochemical characterisation of feeds

The feasibility study of PNS and PS is listed in Table 1, which is comparable with cashew nutshell,[17] pine cone shells,[18] waste groundnut shells,[19] polypropylene,[20] and low-density polyethylene.[21] The proximate analysis of PNS and PS confirmed moisture contents of 5.01% and 0.31%, which are found to be lower than the permissible limits (<10 wt%).[22] PNS has a good agreement with cashew nutshell, which was found to be lower than Pinecone shells and waste groundnut shells. The moisture content plays a crucial role in pyrolysis and biomass processing as it directly affects thermal efficiency, product yield, and energy consumption. Higher moisture levels increase energy demand for drying, reducing overall process efficiency and bio-oil yield while favouring gas and water production. Lower moisture content enhances pyrolysis efficiency by promoting better heat transfer and improving char and liquid fuel yields.[22] Further, PNS and PS confirmed 84.41 and 99.62 wt% volatile matter, 2.30 and 0.05 wt% ash content, and 8.28 and 0.02 wt% fixed carbon. PNS's volatile matter was higher than that of cashew nutshell, pinecone shells, and waste groundnut shells, whereas PS had a good agreement with PP and LDPE. Further, the ash content of PNS is in good agreement with waste groundnut shells and is higher than that of cashew nutshell and pinecone shells.

© 2025 The Author(s). Published by the Royal Society of Chemistry

Open Access Article. Published on 17 November 2025. Downloaded on 2/17/2026 10:41:37 PM. This article is licensed under a Creative Commons Attribution-NonCommercial 3.0 Unported Licence.

Table 1 Physicochemical characterisation of PNS and PS with other feeds[a]

Analysis	PNS	PS	Cashew Nutshell[17]	Pine cone shell[18]	Waste groundnut shells[19]	PP[20]	LDPE[21]
Proximate analysis (wt%, dry basis)							
Moisture content	5.01 ± 0.31	0.31 ± 0.15	5.30	7.90	7.80	—	—
Volatile matter	84.41 ± 2.78	99.62 ± 0.72	84.60	74.85	74.10	99.90	99.50
Ash content	2.30 ± 0.17	0.05 ± 0.07	1.70	0.53	3.80	0.10	—
Fixed carbon	8.28 ± 0.16	0.02 ± 0.01	8.70	16.73	14.30	—	30.5
Ultimate analysis (wt%, dry basis)							
C	48.90 ± 0.21	91.68 ± 0.11	56.56	46.81	46.30	87	75.96
H	6.80 ± 0.12	7.89 ± 0.10	7.58	7.44	5.90	12.50	13.45
N	1 ± 0.01	—	0.63	0.27	1.70	—	—
S	—	—	1.10	<0.10	0.26	0.10	—
O	43.30 ± 0.12	0.43 ± 0.12	23.85	45.43	45.86	0.40	10.59
H/C	1.66	1.03	1.60	1.90	1.52	1.73	0.18
O/C	0.66	0.002	0.31	0.72	0.74	0.0034	0.14
HHV (MJ kg^{-1})	15.27 ± 0.12	42.15 ± 0.11	23.85	20.50	18.90	47.30	41.27
Bulk density (kg m^{-3})	842.59 ± 3.13	256.25 ± 6.24	480.52	650	425.12	—	—
Biochemical analysis (wt%)							
Cellulose	51.22 ± 0.10	—	25.5	—	38.46	—	—
Hemicellulose	22.01 ± 0.11	—	5.23	—	19.20	—	—
Lignin	21.97 ± 0.10	—	14.3	—	26.30	—	—

[a] PP = polypropylene, LDPE = low-density polyethylene, PNS = pistachio nutshell, PS = polystyrene, HHV = higher heating value.

Biomass with higher volatile matter (>80 wt%) and lower ash content (<10 wt%) exhibits easier ignition, making it a more efficient fuel source. A higher volatile content also promotes greater liquid fuel production during pyrolysis. Additionally, lower ash content minimises the risk of furnace or boiler clogging.[23] Furthermore, the reduced ash content in samples enhances the fuel's heating value, as excessive ash would act as a heat sink, thereby lowering combustion efficiency.[23] A fixed carbon content of less than 10 wt% (8.28 and 0.02 wt% for PNS and PS, respectively) during biomass pyrolysis indicates that most of the biomass was converted into volatile compounds, resulting in higher liquid and gas yields while producing minimal char. This suggests efficient thermal decomposition, favouring pyrolysis oil and gas production over solid carbonaceous residue formation.[24]

Further, elemental analysis of PNS and PS has confirmed 48.90 and 91.68 wt% carbon, 6.80 and 7.89 wt% hydrogen, 43.30 and 0.43 wt% oxygen content, respectively. The nitrogen and sulphur content were found to be almost negligible or absent in PNS and PS. PNS's carbon and hydrogen content is in good agreement with pinecone shells and waste groundnut shells, but is lower than that of cashew nut shells. Similarly, the carbon – content of PS was found to be higher than that of PP and LDPE (Table 1). The lower nitrogen and sulfur content limited the formation of SO_x and NO_x emissions during pyrolysis.[24,25] The elemental composition of biomass significantly influences its heating value, with carbon content being directly correlated to the fuel's energy potential.[25] The oxygen content of PNS was found to be 43.30 wt%, which is in good alignment with pinecone shells and waste groundnut shells. Similarly, PS has a good agreement with PP about lower than LDPE. Polypropylene (PP) has a lower oxygen content than low-density polyethylene (LDPE) because of its chemical structure. PP consists solely of carbon and hydrogen, whereas LDPE contains more oxygen-containing impurities due to its manufacturing process. The absence of oxygen in PP enhances its thermal stability and increases its heating value compared to LDPE.[26]

The H/C and O/C ratios of biomass are crucial indicators of fuel quality and pyrolysis efficiency. A higher H/C ratio enhances hydrocarbon formation, thereby improving bio-oil quality, while a lower O/C ratio reduces oxygenated compounds, resulting in a higher energy content. Optimising these ratios helps produce high-quality biofuels with enhanced stability and combustion properties. The molar H/C ratios of PNS and PS were found to be 1.66 and 1.03, which are in good agreement with groundnut shells and cashew nutshells but are lower than that of pinecone shells. Furthermore, the O/C ratios of PNS and PS were found to be 0.66 and 0.002, respectively, which agree with other reported biomass values in Table 1. Fig. 2 illustrates the H/C and O/C ratios of biomass and plastic feedstocks listed in Table 1, indicating their correlation with heating value. As the O/C ratio decreases and the H/C ratio increases, the heating value improves. Plastics (PP and LDPE) exhibit lower O/C and H/C ratios, signifying higher energy potential compared to biomass. The HHV of the PNS and PS was found to be 15.27 and 42.15 MJ kg^{-1}, which holds a good agreement with the listed biomass and plastics. The Higher Heating Value (HHV) is a crucial parameter in biomass pyrolysis as it determines the energy potential of the produced biochar, pyrolysis oil, and syngas. A higher HHV indicates greater energy content, making the fuel more efficient for combustion or further processing. It directly correlates with carbon content and, inversely, with oxygen content, influencing the selection of biomass feedstocks for pyrolysis-based biofuel production.

Open Access Article. Published on 17 November 2025. Downloaded on 2/17/2026 10:41:37 PM.
This article is licensed under a Creative Commons Attribution-NonCommercial 3.0 Unported Licence.

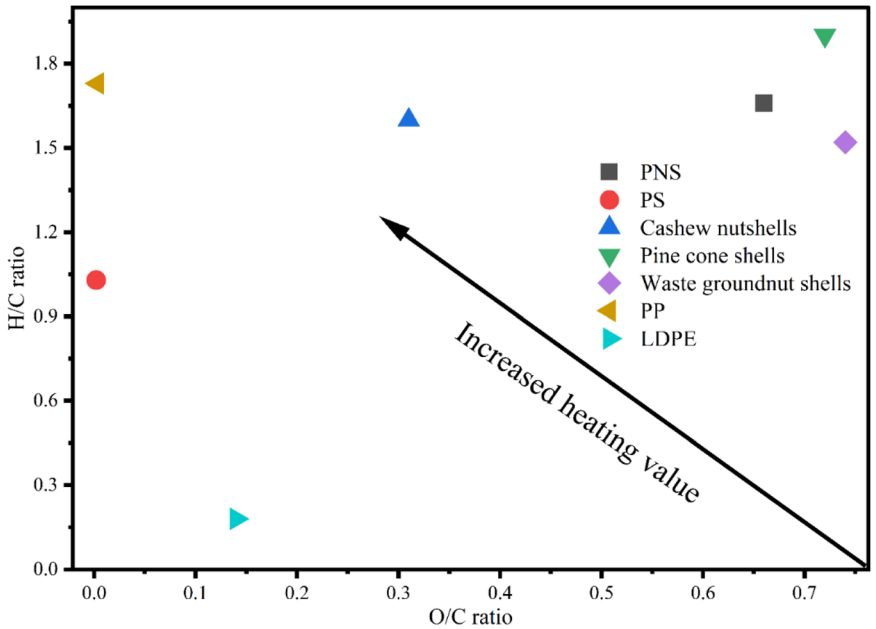

Fig. 2 Van–Krevelen diagram of PNS and PS along with other testified feeds.

Furthermore, the bulk density of PNS and PS was found to be 842.59 and 256.25 kg m^{-3}, respectively. The PNS has a higher bulk density than the cashew nutshell, pine nutshells, and groundnut shells. Bulk density influences the storage, transportation, and processing efficiency of biomass, affecting reactor design, heat transfer, and overall pyrolysis performance. Lastly, the biochemical composition of PNS was confirmed as 51.22 wt% cellulose, 22.01 wt% hemicellulose and 21.97 wt% lignin, which has good agreement with the feeds listed in Table 1. The elevated cellulose and hemicellulose content in PNS suggests a higher liquid fuel yield during pyrolysis.[27]

3.2. Thermal analysis

The thermal stability profiles of PNS and PS at 10 °C min^{-1} were analysed in Fig. 3a and b. It was found that PNS undergoes a multi-step weight loss process, comprising drying, active pyrolysis, and passive pyrolysis stages, whereas PS has only an active decomposition stage (Fig. 3a). The first stage (30–150 °C) is attributed to the removal of the mixture and light volatile matter. In the first stage, PNS and PS were found to be 10.32 and 0.37% which align well with the characterisation data reported in Table 1. Furthermore, the second stage (150–550 °C) confirmed maximum decomposition (67% and 99.63% for PNS and PS), due to the continuous supply of heat. At this stage, the higher-weight compounds fractionate into lower-weight compounds. In contrast, PS shows a sharp, single-step decomposition occurring primarily between 300 and 450 °C, indicating rapid depolymerization and chain scission of the polymer, with almost no char residue remaining after 450 °C.[28] These differences suggest that PS has higher thermal stability up to its degradation point and decomposes more cleanly, while PNS degrades more slowly and leaves behind solid residue. When co-pyrolysed, PS can provide heat and volatiles that facilitate the breakdown of biomass components, potentially enhancing pyrolysis oil yield and modifying product distribution.[28] This thermal behaviour supports the strategic use of PS in biomass pyrolysis to optimise energy transfer and improve process efficiency. The third stage (>550 °C) is known as the char formation stage, which decomposes at a slower rate within a wider temperature range (200–900 °C).[29]

The DTG profiles of PNS and PS are presented in Fig. 3b. For the PNS sample, the first two peaks, appearing at 252 and 332 °C, confirmed the decomposition of hemicellulose and cellulose. However, lignin decomposition does not have any sharp peaks due to the slow decomposition rate. The peak arose at 413 °C for PS, confirming random chain scission, leading to an unzipping reaction that regenerates the styrene monomer, which is the main decomposition product.[28] This process is highly efficient, resulting in the rapid volatilisation of the polymer into low-molecular-weight compounds, including styrene, along with minor products such as benzene, toluene, ethylbenzene, and other light aromatic hydrocarbons.[30] It is noteworthy that PS does not contain oxygenated functional groups or inorganic matter, so its decomposition leaves almost no solid residue or char.[28] The sharp and intense weight loss peak in this temperature range confirms the fast and complete breakdown of PS, making it thermally less complex but highly volatile. This characteristic makes PS a suitable co-feed in pyrolysis processes, as its decomposition can supply both heat and reactive volatiles to enhance the thermal conversion of biomass. The fixed carbon value of PS reported in Table 1 supported the TGA results of PS.[30]

3.3. FTIR analysis

FTIR analysis of PNS and PS (Fig. 4) confirmed the presence of various functional groups. In the case of PNS, the broad

© 2025 The Author(s). Published by the Royal Society of Chemistry

Open Access Article. Published on 17 November 2025. Downloaded on 2/17/2026 10:41:37 PM.
This article is licensed under a Creative Commons Attribution-NonCommercial 3.0 Unported Licence.

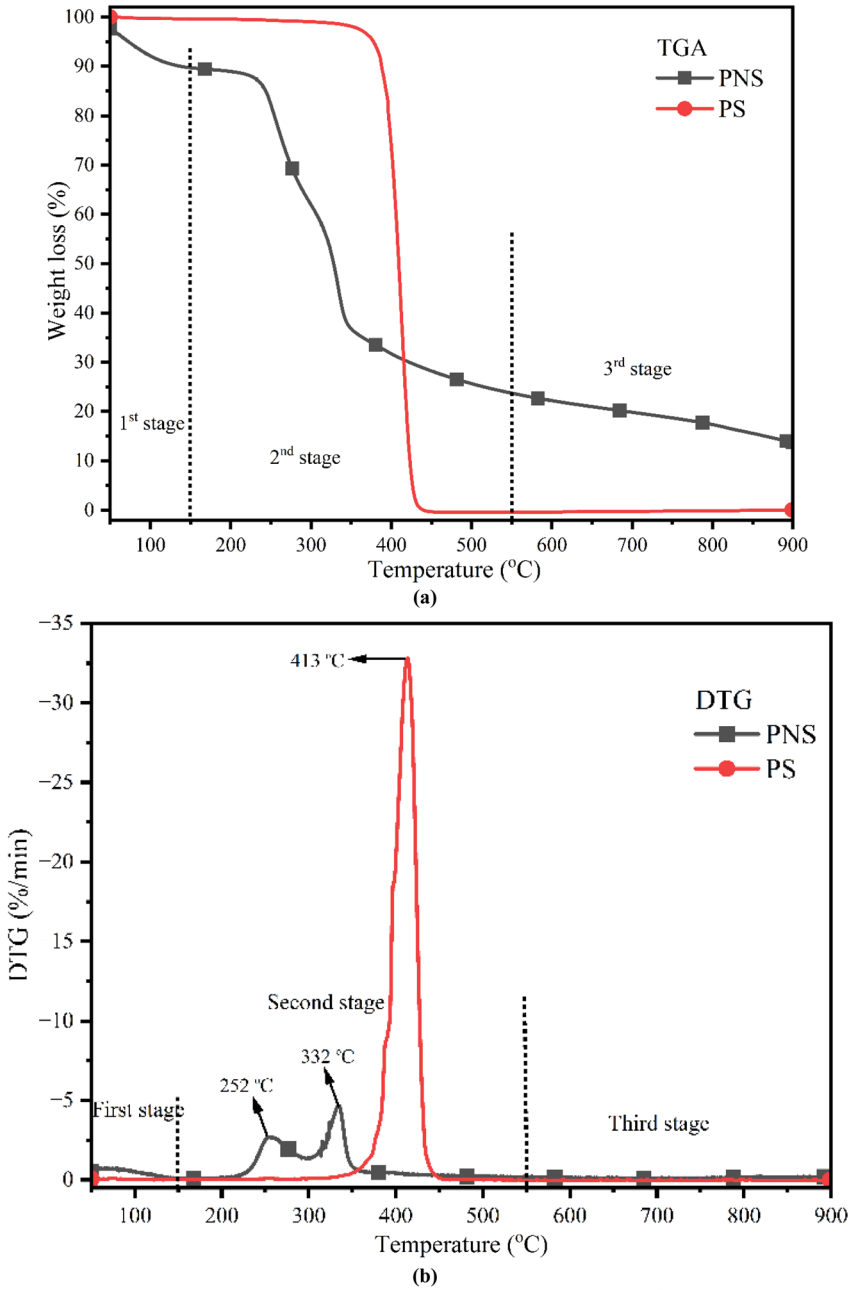

Fig. 3 Thermal analysis of (a) PNS and (b) PS at 10 °C min^{-1} heating rate.

absorption band between 3000–3500 cm^{-1} (centred at 3328 cm^{-1}) corresponded to –OH stretching vibrations, indicating the presence of water, phenols, alcohols, acids, and proteins.[31,32] The peak at 2920 cm^{-1} was attributed to CH_2 and CH_3 asymmetric and symmetric stretching, suggesting alkenes and carboxylic acids.[31] Absorptions in the range of 1620–1730 cm^{-1} confirmed carbonyl (C=O) groups, primarily ketones and esters.[33] Peaks between 1230–1407 cm^{-1} indicated methyl and phenolic groups, while those at 1000–1042 cm^{-1} suggested ethers and esters due to C–O stretching.[23,34] Finally, the region between 650–900 cm^{-1} confirmed the presence of mono- and substituted aromatic compounds.[34,35] FTIR analysis of PS revealed characteristic absorption bands indicative of its chemical structure. Bands observed at 3871, 3668, 3311 cm^{-1}, 1339 cm^{-1}, and around 550 cm^{-1} corresponded to aromatic and substituted phenyl rings.[36] The peak at 2851 cm^{-1} was attributed to C–H and =C–H stretching vibrations, confirming the presence of alkanes and alkenes.[31] Peaks at 1565 cm^{-1} and in the range of 1750–1850 cm^{-1} were associated with C=C stretching, indicating the presence of carbon–carbon double bonds. Additionally, the peak at 2917 cm^{-1} corresponded to C–H stretching in $-CH_3$ or $-CH_2^-$ groups.[36] Furthermore, peaks in 2015, 1816, and 1009 cm^{-1} were linked to symmetric, asymmetric, and deformation vibrations of C–H bonds, confirming the presence of aromatic compounds.[37]

© 2025 The Author(s). Published by the Royal Society of Chemistry

Open Access Article. Published on 17 November 2025. Downloaded on 2/17/2026 10:41:37 PM.
This article is licensed under a Creative Commons Attribution-NonCommercial 3.0 Unported Licence.

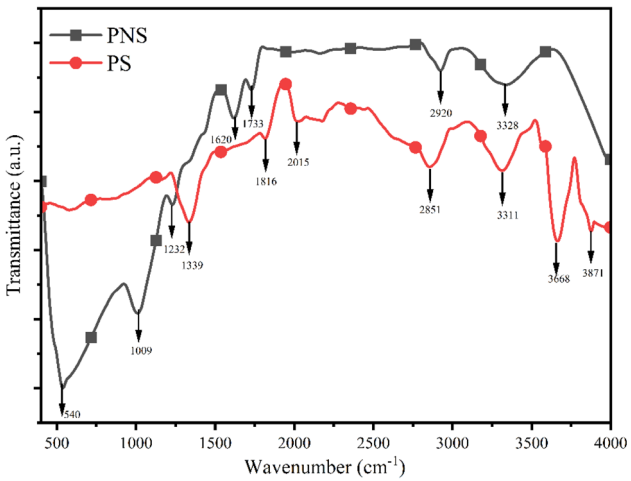

Fig. 4 FTIR analysis of PNS and PS.

3.4. Process parameters optimisation

3.4.1. Effect of temperature. Temperature greatly affects biomass pyrolysis by influencing product distribution and yield. Higher temperatures favour bio-oil and gas production, while lower temperatures enhance biochar yield.[38] It also impacts reaction rates, devolatilization, and secondary reactions. Optimal temperature selection is crucial to maximising desired products and improving the overall efficiency of the pyrolysis process. The pyrolysis experiments were conducted at temperatures of 500, 550, 600, and 650 °C to determine the optimal conditions for maximum liquid yield and to analyse the properties of the resulting pyrolysis oil. As shown in Fig. 5, the highest oil yield (40.05 wt%) was obtained at 550 °C, accompanied by 28.12 wt% char and 33.58 wt% syngas. This indicates that 550 °C is the optimal temperature for maximising the liquid fraction, as it achieves an ideal balance between primary decomposition and secondary vapour cracking reactions. At this temperature, sufficient thermal energy is provided to decompose lignocellulosic components cellulose, hemicellulose, and lignin into volatile intermediates, which subsequently condense into liquid oil upon cooling. The dominance of depolymerisation and decarboxylation reactions in this range leads to higher volatile evolution and minimised secondary gas formation, enhancing liquid yield. Furthermore, at 500 °C, the yields of pyrolysis oil, char, and syngas were observed to be 38.34 wt%, 27.78 wt%, and 33.86 wt%, respectively. At higher temperatures of 600 °C and 650 °C, the pyrolysis oil yields slightly increased to 38.69 wt% and then decreased to 36.23 wt%, while char yields were 28.93 wt% and 26.39 wt%, and syngas yields were 31.01 wt% and 33.37 wt%, respectively. This reduction in pyrolysis oil production at elevated temperatures can be attributed to intensified secondary cracking reactions and reforming processes, which break down heavier organic vapours into lighter, non-condensable gases such as CO, CO_2, CH_4, and H_2.[39] The higher thermal energy at these conditions favours gas-phase reactions over condensation, converting volatile intermediates into permanent gases rather than condensable liquids. In addition, thermal polymerisation of reactive tar vapours may lead to the formation of solid carbonaceous residues, further reducing oil yield.[40]

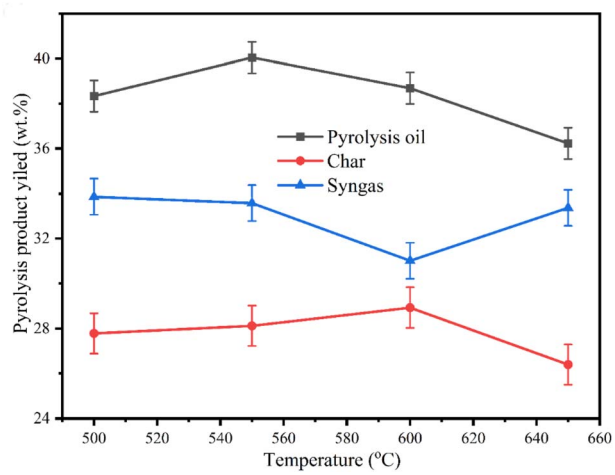

Fig. 5 Effect of pyrolysis temperature on pyrolysis oil yield.

The char yield trend displays a relatively stable behaviour up to 550 °C, followed by a slight increase at 600 °C and a decline at 650 °C. Initially, the char yield increases marginally due to incomplete devolatilization at lower temperatures. As the temperature rises, primary decomposition becomes more extensive, leading to lower char residues. The slight rise around 600 °C might be associated with secondary condensation of heavy vapours on char surfaces or the formation of polyaromatic carbonaceous structures through repolymerization reactions.[39] However, above 600 °C, char yield drops significantly to 26.39 wt%, signifying more complete volatilization and enhanced conversion of solid carbon to gas. This decline indicates that higher temperatures favour thermal cracking and gasification reactions, reducing the solid residue and improving the overall conversion efficiency of the biomass feed.[39] The syngas yield, indicated by the blue line, exhibits an inverse relationship with the yields of char and oil. It remains nearly constant at around 33 wt% between 500 °C and 550 °C, decreases slightly to about 31.01 wt% at 600 °C, and then rises sharply to 33.37 wt% at 650 °C. The initial stability of the gas yield corresponds to the equilibrium between volatile evolution and condensation reactions. The slight dip near 600 °C may be due to partial condensation of light hydrocarbons or temporary stabilisation of intermediates.[41] The subsequent increase in gas yield at higher temperatures results from intensified secondary cracking and gasification reactions that convert condensable vapors and char into gaseous products. Reactions such as decarboxylation, decarbonylation, and reforming of hydrocarbons become dominant, promoting the formation of CO, CO_2, and H_2 at elevated temperatures.[41] The maximum pyrolysis oil yield at 550 °C is due to the optimal balance between thermal decomposition and secondary cracking. At this temperature, biomass breaks down efficiently into volatiles that condense into liquid oil. However, lower temperatures (500 °C) cause incomplete decomposition, while higher temperatures (600–650 °C) promote secondary reactions, converting volatiles into non-condensable gases, thereby reducing oil yield by 41%.

© 2025 The Author(s). Published by the Royal Society of Chemistry

Open Access Article. Published on 17 November 2025. Downloaded on 2/17/2026 10:41:37 PM.
This article is licensed under a Creative Commons Attribution-NonCommercial 3.0 Unported Licence.

3.4.2. Effect of plastic loading. Plastic loading significantly influences pyrolysis oil yield by enhancing the volatile content and hydrogen availability during co-pyrolysis with biomass. Moderate plastic addition can improve oil quality and yield due to synergistic interactions. However, excessive plastic loading may lead to increased gas formation and reduced liquid yield due to secondary cracking.[42] The effect of increasing plastic (PS) loading on the pyrolysis of PNS is clearly observed in the product yield distribution (Fig. 6). During thermal pyrolysis of PNS, the pyrolysis oil yield was approximately 40 wt%, with char and syngas yields at around 28 wt% and 34 wt%, respectively. Upon introducing 20 wt% PS, the pyrolysis oil yield increased significantly to approximately 47.59 wt%, while the char and syngas yields dropped to about 23.31 wt% and 31.01 wt%. Further increasing the PS content to 30 wt% resulted in a continued rise in pyrolysis oil yield to approximately 51.46 wt%, accompanied by reduced char (21.54 wt%) and syngas (27 wt%) production. Furthermore, at the highest plastic loading of 50 wt%, a maximum pyrolysis oil yield of approximately 53.51 wt% was achieved, while the char yield increased slightly to 24.09 wt%, and the syngas yield decreased to 22 wt%, respectively. Although 50 wt% plastic loading resulted in the highest pyrolysis oil yield (53.51 wt%), the oil produced was highly viscous, causing blockage in the condenser during the experiment. Therefore, in this study, 30 wt% PS loading was considered the optimal level for efficient and stable pyrolysis operation. These results indicate that increasing PS content enhances liquid product formation due to improved volatile release and synergistic interactions while simultaneously reducing solid and gaseous by-products.

The effect of plastic loading on pyrolysis product distribution is influenced by the inherent properties of polystyrene (PS), which has a high volatile and hydrogen content compared to biomass. The increasing PS content in the PNS feedstock results in a 13.46% increase in pyrolysis oil yield, while the yields of char and syngas decline. This enhancement in oil production is primarily due to synergistic interactions between the biomass and plastic during co-pyrolysis. Polystyrene decomposes readily into low-molecular-weight hydrocarbons, providing additional hydrogen that stabilises reactive intermediates and suppresses secondary cracking reactions. This results in higher liquid yield and improved oil quality.[43] Moreover, the presence of PS promotes the breakdown of heavy biomass components into more condensable volatiles, further boosting oil production.[42] At the same time, the decrease in char yield is attributed to complete volatilization of the feedstock, while reduced syngas formation occurs due to the redirection of volatile intermediates into liquid products instead of further cracking into non-condensable gases.[43] Thus, the co-pyrolysis process becomes more favourable for liquid fuel production with increasing plastic content.

3.4.3. Effect of the feed to catalyst ratio. The introduction of CuO has a significant influence on pyrolysis, enhancing reaction rates and altering product distribution. Additionally, catalysts promote secondary cracking, which reduces the yield of pyrolysis oil while increasing the formation of gas and char. Results suggested a reduced yield of pyrolysis oil, but the use of CuO improves pyrolysis oil quality by reducing oxygenated compounds, and making it more stable and energy-dense for fuel applications.[44] Fig. 7 shows the impact of CuO loading on the pyrolysis product distribution of PNS blended with 30 wt% PS. Thermal pyrolysis (PNS + PS 30 wt%) oil yield peaked at approximately 51.46 wt%, significantly higher than that of raw PNS (40 wt%), due to the synergistic effect of PS and PNS. However, the addition of CuO further led to a decline in pyrolysis oil yield to around 47.23 wt% at 5 wt% and an additional 41.26 wt% at 10 wt% CuO. Simultaneously, char yield increased from about 21 to 27 wt%, while syngas yield rose from 27 to 32 wt%, respectively. This trend suggests that CuO acts as a catalyst, promoting cracking and gasification reactions that convert more volatiles into non-condensable gases and solid residues, thereby reducing the liquid yield by 45%. The catalytic activity of CuO facilitates dehydrogenation, decarboxylation, and reforming reactions, enhancing syngas formation while also promoting the formation of more stable char structures.[44]

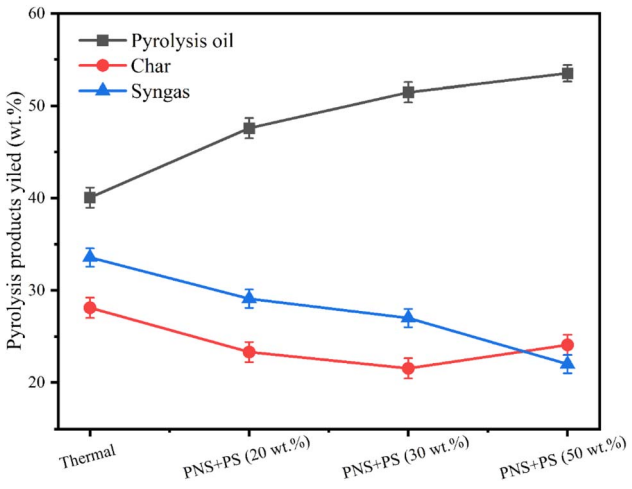

Fig. 6 Effect of plastic loading on pyrolysis oil yield.

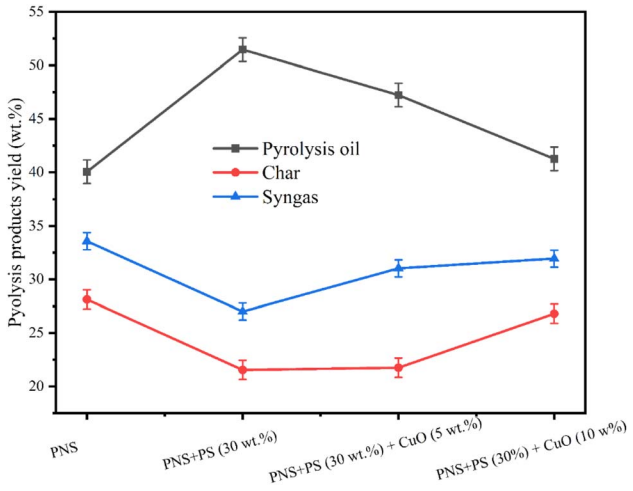

Fig. 7 Effect of the biomass-to-plastic-to-catalyst ratio on pyrolysis product yield.

Open Access Article. Published on 17 November 2025. Downloaded on 2/17/2026 10:41:37 PM. This article is licensed under a Creative Commons Attribution-NonCommercial 3.0 Unported Licence.

Therefore, while plastic addition initially boosts pyrolysis oil yield, increasing CuO loading shifts the product distribution toward more gas and char at the expense of pyrolysis oil.[45,46]

3.5. Physicochemical characterisation of pyrolysis oil

The physicochemical characterisation of pyrolysis oil is listed in Table 2 and compared with other tested pyrolysis oils. The comparative analysis of pyrolysis oils derived from biomass and plastic blends, with and without catalytic, reveals significant variations in physicochemical properties that directly influence their fuel quality and potential application. Thermal pyrolysis oil has a brown colour, smoky odour, and exhibits moderate carbon (58.98%), hydrogen (6.86%), negligible nitrogen (0.78%), and a high oxygen (33.38%), leading to an H/C ratio of 1.39 and an O/C ratio of 0.42. Further, the higher heating value (HHV) is relatively low (25.70 MJ kg^{-1}) compared to other pyrolysis oils in Table 2, indicating limited energy density, while it has a higher density (1028.42 kg m^{-3}), viscosity (77.25 cP), and pH (2.29). The physicochemical characterisation of thermal oil highlighted several limitations that hinder its direct use as a transportation fuel, indicating the need for further upgrading. Thermal pyrolysis oil hinders its direct use as a transportation fuel, as it has high oxygen content (33.38%), which results in low energy density, chemical instability, and poor combustion characteristics.[47] The thermal pyrolysis oil exhibits a relatively lower heating value (25.70 MJ kg^{-1}), which means it produces less energy per unit compared to conventional fuels.

Furthermore, its high viscosity (77.25 cP at 35 °C) poses challenges for fuel injection and atomization in engines, while its high acidity (pH 2.29) can cause corrosion in engine and fuel storage systems.[48] Additionally, the higher fuel density (1028.42 kg m^{-3}) and elevated oxygen-to-carbon ratio (O/C = 0.42) indicate incomplete deoxygenation, which reduces its fuel quality. The low carbon content (58.98%) further compromises its calorific value, and the smoky odour and dark colour suggest the presence of heavy, potentially harmful compounds.[47,48] PS was blended with PNS at 30 wt%, resulting in pyrolysis oil that turned blackish brown and showed an increase in carbon content (68.69%) and a decrease in oxygen (23.50%), enhancing HHV (30.06 MJ kg^{-1}). This composition also improved fuel characteristics by reducing fuel density (954.85 kg m^{-3}) and viscosity (42.61 cP), with a less acidic pH (3.10). Blending plastics at 30 wt% with biomass significantly improved the fuel characteristics of the resulting pyrolysis oil due to the high carbon and hydrogen content and low oxygen content inherent in plastics like polystyrene.[47] This blend led to an increase in carbon content (from 58.98% to 68.69%), a reduction in oxygen content (from 33.38% to 23.50%), and an enhanced higher heating value (from 25.70 MJ kg^{-1} to 30.06 MJ kg^{-1}), indicating improved energy density.[3] Additionally, the blend of plastics (PS) lowered the viscosity (from 77.25 to 42.61 cP) and reduced acidity (pH increased from 2.29 to 3.10), contributing to better fuel handling and reduced corrosiveness.[3] These enhancements result from the thermal degradation of plastics, producing more hydrocarbons and fewer oxygenated compounds, thereby improving the overall quality, stability, and combustion performance of the pyrolysis oil.[47,49]

The addition of CuO at 5 wt% to the PNS + PS blend during pyrolysis enhanced the fuel properties of the resulting oil by acting as a catalyst that promotes deoxygenation, cracking of heavy molecules, and formation of hydrocarbon-rich compounds.[50] This catalytic effect led to a significant increase in carbon content (from 68.69% to 79.40%) and a marked reduction in oxygen content (from 23.50% to 11.69%), which collectively boosted the higher heating value from 30.06 MJ kg^{-1} to 35.90 MJ kg^{-1}, indicating superior energy density.[45] Furthermore, CuO reduced the viscosity (from 42.61 to 36.40 cP), lowered ash content (to 0.082%), and slightly increased the pH (to 3.27), which contributes to improved combustion performance, reduced corrosiveness, and enhanced fuel handling. These improvements result from CuO ability to facilitate secondary reactions, break oxygenated bonds, and suppress the formation of polar compounds, thereby producing a cleaner, more stable, and energy-dense bio-oil.[45] Furthermore, BGS shows a lower carbon content (52.90%), the highest H/C

Table 2 Physicochemical analysis of pyrolysis oil and comparison with other pyrolysis oils

Analysis	Thermal pyrolysis oil	PNS + PS (30 wt%) pyrolysis oil	PNS + PS (30 wt%) + CuO (5 wt%) pyrolysis oil	BGS[52]	SNS[52]	CNS + PS[53]
Colour	Brown	Blackish brown	Blackish brown			
Odour	Smoky	Smoky	Smoky			
Elemental analysis (wt%)						
C	58.98 ± 0.12	68.69 ± 0.11	79.40 ± 0.14	52.90	63.30	64.94
H	6.86 ± 0.10	7.33 ± 0.10	7.70 ± 0.10	8.00	08.30	7.96
N	0.78 ± 0.10	0.48 ± 0.10	1.21 ± 0.10	00.90	01.60	0.07
S	—	—	—	0.04	00.20	0.26
O	33.38 ± 0.12	23.50 ± 0.14	11.69 ± 0.17	37.80	26.60	26.98
H/C	1.39	1.19	1.16	1.81	1.57	1.47
O/C	0.42	0.34	0.11	0.53	0.31	0.31
HHV (MJ kg^{-1})	25.70 ± 0.10	30.06 ± 0.10	35.90 ± 0.10	23.7 ± 1.8	26.5 ± 2.0	31.38
Ash content	1.01 ± 0.81	0.80 ± 0.94	0.082 ± 0.31	—	—	0.05
Density (kg m^{-3})	1028.42 ± 0.38	954.85 ± 0.44	952.65 ± 0.46	1.01 ± 0.0	1.04 ± 0.0	0.945
Viscosity at 35 °C at 100 RPM	77.25 ± 0.14	42.61 ± 0.12	36.40 ± 0.10	—	—	48
pH	2.29 ± 0.10	3.10 ± 0.10	3.27 ± 0.10	5.01	2.87	3.8

© 2025 The Author(s). Published by the Royal Society of Chemistry

Open Access Article. Published on 17 November 2025. Downloaded on 2/17/2026 10:41:37 PM.
This article is licensed under a Creative Commons Attribution-NonCommercial 3.0 Unported Licence.

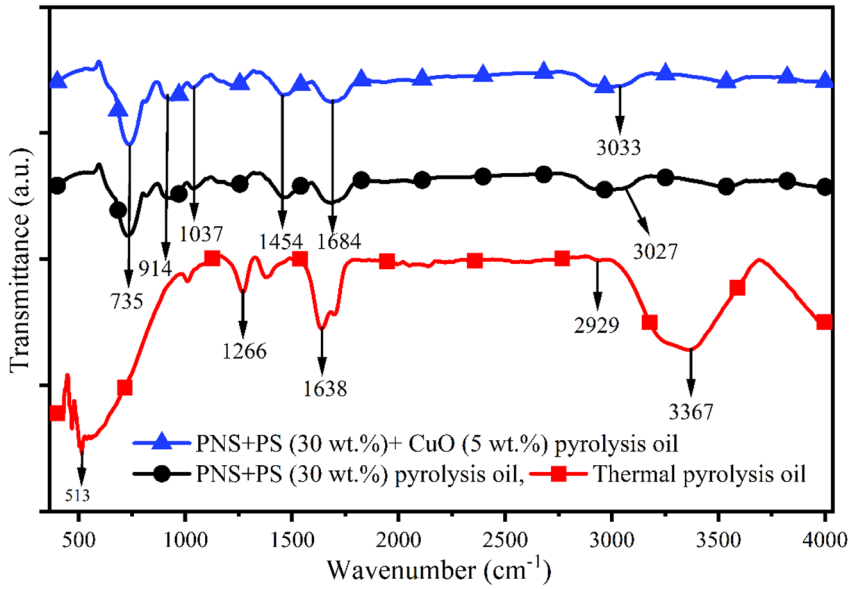

Fig. 8 FTIR analysis of pyrolysis oil obtained from pyrolysis at 550 °C.

ratio (1.81), but the lowest HHV (23.7 MJ kg^{-1}), indicating lower energy density. SNS displays relatively balanced characteristics with a carbon content of 63.30%, oxygen at 26.60%, and an HHV of 26.5 MJ kg^{-1}, while CNS + PS blend oil shows decent performance with 64.94% carbon, a lower O/C ratio (0.31), and an HHV of 31.38 MJ kg^{-1} (Table 2). The use of CuO with PNS + PS blends pyrolysis oil exhibited the best performance in terms of energy content, elemental composition, and physicochemical properties such as low viscosity, density, and ash content (0.082%), indicating efficient conversion and greater fuel quality.[50] This suggests that the integration of polystyrene into biomass significantly enhances carbon content and fuel properties, while the use of CuO further promotes deoxygenation and energy densification of pyrolysis oils. The data underscores the potential of tailored feedstock and catalyst optimisation strategies in producing high-grade bio-oils suitable for advanced fuel applications, outperforming conventional biomass pyrolysis oils and even some co-pyrolysis products reported in the literature.[51] Overall, the results emphasise the effectiveness of combining plastic waste with lignocellulosic biomass under catalytic pyrolysis to yield pyrolysis oil with improved HHV, stability, and combustion characteristics.[45]

3.6. FTIR analysis of pyrolysis oil

FTIR analysis of the thermal, co-pyrolysis and catalytic pyrolysis oil provides insights into the functional groups, indicating the nature of the organic compounds generated during pyrolysis (Fig. 8). The thermal pyrolysis oil displayed distinct absorption bands at 513 cm^{-1}, corresponding to C–Cl stretching vibrations, and 735 cm^{-1}, likely associated with out-of-plane C–H bending of aromatic compounds.[54] The peaks at 1266 cm^{-1} and 1684 cm^{-1} indicate the presence of C–O stretching in esters and C=O stretching in carbonyl groups, respectively, suggesting the presence of ketones or aldehydes.[55] The broad absorption around 2929 cm^{-1} is characteristic of C–H stretching in aliphatic hydrocarbons, while the broad peak at 3367 cm^{-1} is assigned to O–H stretching, possibly due to alcohols or phenolic compounds.[56] Further, PNS + PS (30 wt%) pyrolysis oil at 735 and 3027 cm^{-1} indicates aromatic ring deformations and unsaturated C–H stretching, respectively. These functional groups point to the presence of aromatic hydrocarbons and unsaturated compounds.[57] Interestingly, the catalytic pyrolysis oil using CuO exhibited minimal transmittance changes, with weaker or nearly absent peaks, especially in the carbonyl and hydroxyl regions.[53] This implies that the CuO may facilitate more complete cracking or deoxygenation of oxygenated compounds, resulting in a cleaner oil with reduced polar functionalities.[55] Overall, FTIR spectra confirm the presence of diverse organic functionalities, including aliphatic, aromatic, carbonyl, and hydroxyl groups, with compositional variations influenced by feedstock ratios and catalytic conditions.

3.7. NMR analysis of pyrolysis oil

An overview of the entire content of the pyrolysis oil was obtained through structural characterisation using ^{1}H NMR. A semi-quantitative evaluation of hydrogen atoms of oxygenated compounds and hydrocarbons was obtained by integrating the relevant spectra regions, removing the solvent residual signal (2.4 ppm) and the water signal (3.7–3.3 ppm).[58] ^{1}H NMR spectra of PNS, PS, PNS + PS (30 wt%) and PNS + PS (30 wt%)+CuO (5 wt%) are displayed in Fig. 9a–c. Furthermore, the integrated signal areas for each sample at various ppm values are listed in Table 3. From the result, it was noticed that the area of COOH (11–12.50 ppm) was slightly increased by the addition of PS (30 wt%) and decreased by the addition of CuO (30 wt%), respectively. The GC-MS composition also confirms the similar trends for acid alterations. Furthermore, the area of CHO, ArOH (8.2–11.0 ppm) confirmed a reduction in phenols and aldehyde,

Open Access Article. Published on 17 November 2025. Downloaded on 2/17/2026 10:41:37 PM.
This article is licensed under a Creative Commons Attribution-NonCommercial 3.0 Unported Licence.

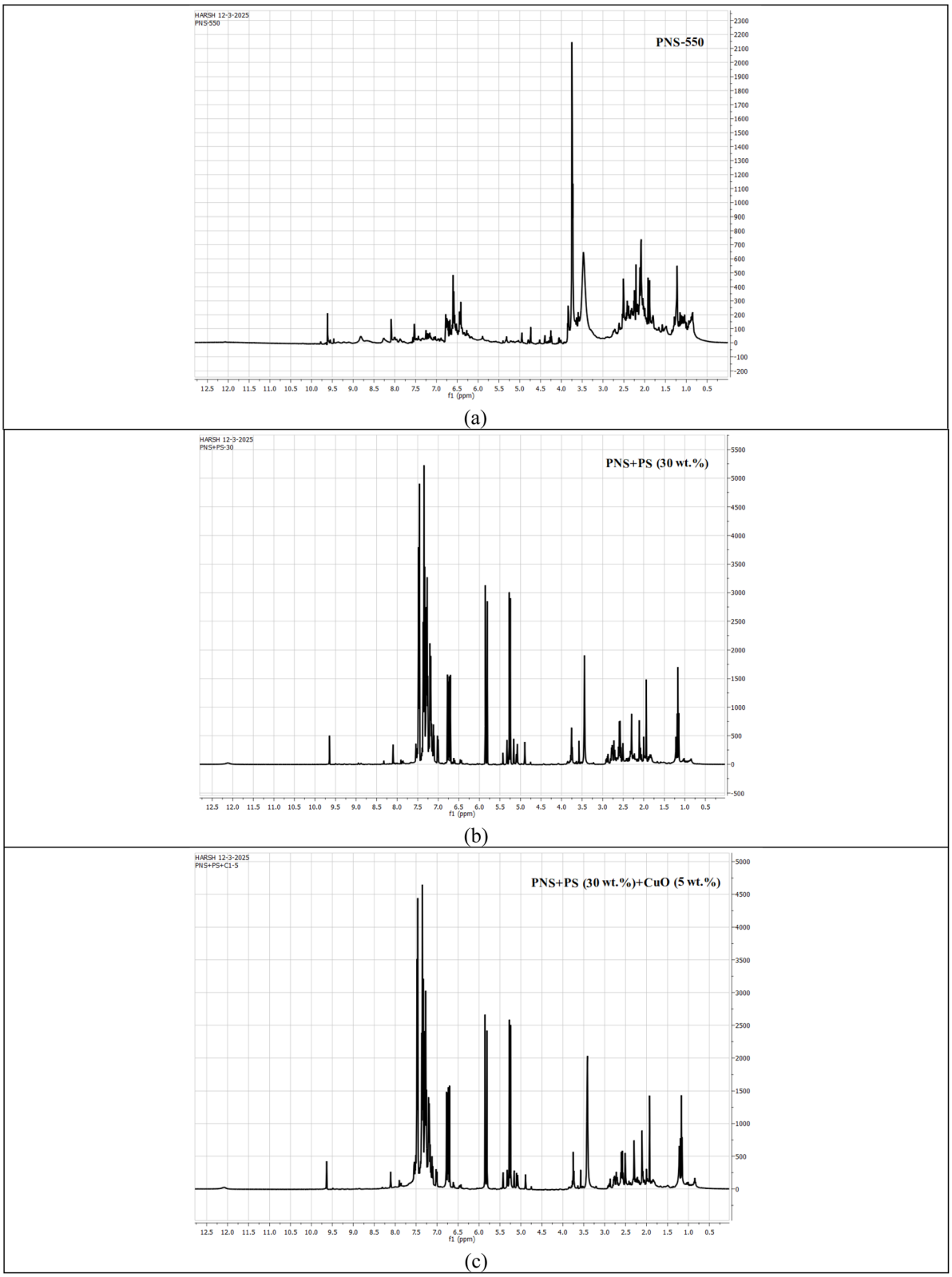

Fig. 9 ^{1}H NMR spectra of pyrolysis oil (a) PNS, (b) PNS + PS (30 wt%) and (c) PNS + PS (30 wt%)+CuO (5 wt%).

which is supported by GC-MS data. The abundance of aromatic and conjugated alkene hydrogens (8.2–6.0 ppm) was found to be increased by the addition of PS and CuO.[58] It is challenging to evaluate the behaviour of carbonyl species' hydrogens due to the spectral overlap of aliphatic and carbonyl hydrogens. However, compared to thermal pyrolysis, hydrogen percentages

© 2025 The Author(s). Published by the Royal Society of Chemistry

Open Access Article. Published on 17 November 2025. Downloaded on 2/17/2026 10:41:37 PM. This article is licensed under a Creative Commons Attribution-NonCommercial 3.0 Unported Licence.

Table 3 Percentage (%) of hydrogen based on ^{1}H NMR analyses of bio-oils grouped according to chemical shift range[a]

Chemical shift (ppm)	Hydrogen assignment	PNS	PNS + PS (30 wt%)	PNS + PS (30 wt%) + CuO (5 wt%)
12.5–11.0	COOH	0.25	0.27	0.21
11.0–8.2	CHO, ArOH	0.86	0.20	0.20
8.2–6.0	Aromatic and conjugated H	14.58	50.14	55.61
6.0–4.20	Aliphatic OH, =CH=CH=, Ar=CH_2 + O=R	2.53	10.31	10.58
4.2–3.0	R–CH_2–O–R, CH_3–O–R	25.95	6.08	7.58
3.0–2.0	–CH_2CH=O, aliphatic H	25.59	12.68	11.67
2.0–0.0	Aliphatic H	24.70	20.29	14.23

[a] Excluding the water (3.7–3.3 ppm) and the solvent residual signals (2.4 ppm).

in the 3.0–0.0 ppm range show a slight decrease in aliphatic hydrogens when employing a PS and CuO catalyst.[59] The pyrolysis oil indicates a substantial reduction in hydrogens associated with ethers (4.2–3.0 ppm) due to the introduction of PS and CuO. This phenomenon happens due to structural transformation or degradation of ether linkages. Further, CuO acts as a catalyst, promoting cleavage or reduction reactions, while PS may hinder ether formation or alter the chemical environment.[60] Further, the Aliphatic OH, =CH=CH=, Ar=CH_2 + O=R (4.2–6.0 ppm) was found to be increased by the addition of PS and CuO. The increase in aliphatic with PS and CuO addition suggests enhanced formation of unsaturated and oxygenated compounds. CuO likely promotes oxidation and dehydrogenation, while PS contributes additional carbon sources and reactive intermediates, facilitating the formation of alcohols, alkenes, and aromatic derivatives through catalytic and thermal interactions.[51] The ^{1}H NMR analysis of pyrolysis oil was supported by GC-MS data. Overall, it was noticed that the use of PS and CuO with PNS resulted in a reduction in oxygenated compounds and an increase in hydrocarbons (aromatic and aliphatic). The formation of aromatic and poly-aromatic hydrocarbons was explained by secondary reactions during pyrolysis, based on Diels–Alder and deoxygenation of oxygenated aromatic compounds mechanisms.[59–61]

3.8. GC-MS analysis

The composition analysis of pyrolysis oil was performed using a GC-MS analyser, and the derived compounds are listed in Fig. 10a and Table S2. Furthermore, the GC-MS spectra obtained from the test are listed in Fig. 10b–d. GC-MS results confirmed the existence of phenols, hydrocarbons, acids, alcohols, furan derivatives, nitrogen-containing and cyclo-oxygenated compounds. Significant compositional changes in the pyrolysis oil were revealed by GC-MS analysis due to the addition of polystyrene (PS) and CuO on PNS. The thermal pyrolysis oil confirmed 15.56% phenols, 23.77% hydrocarbons, 7.87% acids, 12.27% alcohols, 1.52 nitrogen-containing compounds, 0.89% furan-based compounds and 3.83% cyclo-oxygenated compounds. However, with the addition of PS at 30 wt% and CuO at 5 wt%, the phenol content was reduced by 9% and 9.7% respectively. The reduction in phenol content is attributed to the dilution of lignin-derived precursors by the catalytic activity of PS and CuO. CuO promotes deoxygenation and aromatic ring cleavage, converting phenols into hydrocarbons and other low-oxygen compounds, thereby lowering the phenol yield by 51%. Furthermore, the hydrocarbon concentration in pyrolysis oil was found to increase by 10.21% and 17.90% with the addition of PS and CuO, respectively, due to enhanced deoxygenation and cracking processes. The catalytic activity of CuO encourages the formation of hydrocarbons, and PS's hydrogen-rich structure is responsible for this increase.[51] On the other hand, the acid concentration in pyrolysis oil was found to be increased by 5.83% and reduced by 2.66% due to the addition of PS and CuO at 30 and 5 wt% due to incomplete deoxygenation and formation of oxygenates during PS thermal breakdown. However, CuO catalyses decarboxylation and deoxygenation, converting acids into CO_2 or hydrocarbons, thereby decreasing acid concentration in the pyrolysis oil.[62] Further, the alcohol content in pyrolysis oil was found to be decreased by 8.96% and 9.56% due to the addition of PS and CuO at 30 and 5 wt%, respectively, due to two main reasons: PS reduces the relative contribution of biomass-derived oxygenates by dilution, while CuO catalyses dehydration and deoxygenation reactions, converting alcohols into alkenes, ethers, or hydrocarbons, thus lowering alcohol levels in the pyrolysis oil.[46]

The nitrogen-containing and cyclo-oxygenated compounds in pyrolysis oil were found to be increased by (0.74 and 0.16%) and 1.51 and 3.27%) due to the addition of PS and CuO at 30 and 5 wt. loading. The slight increase in nitrogen-containing compounds (0.74% with PS and 1.51% with CuO) may result from secondary reactions between PS-derived intermediates and trace nitrogen in the PNS, forming stable nitrogenous compounds. Meanwhile, the notable rise in cyclo-oxygenated compounds (0.16% with PS and 3.27% with CuO) is attributed to the enhanced stabilisation and cyclisation of oxygenated intermediates.[63] PS decomposition may generate aromatic radicals that facilitate ring formation, while CuO acts as a catalyst, promoting oxidative cyclisation and stabilisation of intermediates into oxygen-containing heterocycles.[46,51] Finally, furan-based compounds were found to decrease by 0.16% by the addition of PS at 30 wt%, while using CuO at 5 wt% further increased it by 0.11%, respectively. The slight decrease of 0.16% in furan-based compounds with 30 wt% PS addition is due to the dilution of cellulose and hemicellulose-derived precursors, as PS does not contribute to furan formation. However, the subsequent 0.11% increase with 5 wt% CuO addition is attributed to the catalytic role of CuO in stabilising and promoting

Open Access Article. Published on 17 November 2025. Downloaded on 2/17/2026 10:41:37 PM.
This article is licensed under a Creative Commons Attribution-NonCommercial 3.0 Unported Licence.

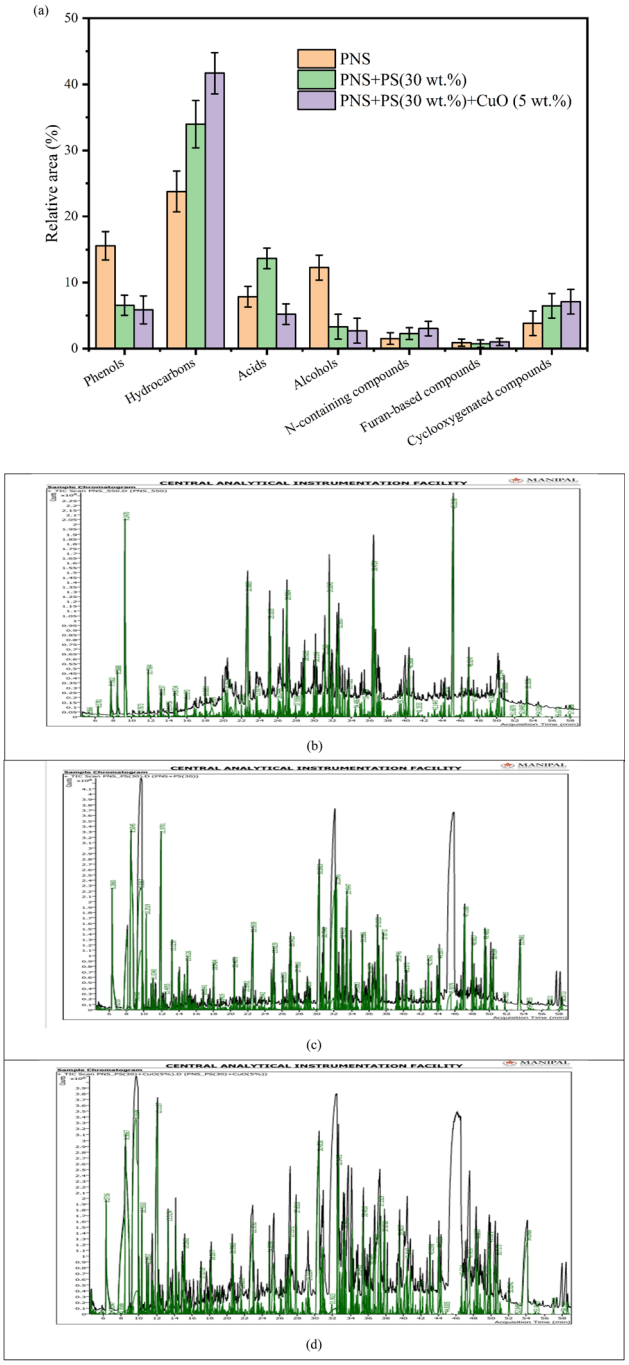

Fig. 10 (a) The compositional analysis of pyrolysis oil derived from GC-MS. GC-MS chromatograph obtained from pyrolysis oil, (b) PNS, (c) PNS + PS (30 wt%) and (d) PNS + PS (30 wt%) + CuO (5 wt%).

the formation of furan derivatives from oxygenated intermediates, enhancing their presence in the pyrolysis oil despite the reduced biomass fraction.[63] Overall, the combined action of PS and CuO at 30 and 5 wt% greatly improves the quality of the pyrolysis oil by suppressing unwanted polar oxygenates and increasing hydrocarbon selectivity.

3.9. Characterisation of char

The char obtained at 550 °C was characterised as per its physical and chemical properties and compared with other chars such as Bambara Groundnut Shell (BGS) and Shea Nutshell (SNS)[52] and presented in Table 4. Table 4 presents a comparative physicochemical analysis of various biochar samples, including PNSC and PNSC blended with 30 wt% PSC. It is evident that the moisture content of chars was found to be below 1% which makes it an ideal candidate for fuel and energy materials.[64] Further, moisture content significantly influences the energy efficiency of char, combustion behaviour, and storage stability. The lower moisture content below 1% enhances calorific value, reduces smoke during burning, and prevents microbial degradation, whereas higher moisture content lowers thermal efficiency, increases drying costs, and limits the effectiveness of char as a fuel or soil amendment.[64] Further, carbon content significantly increases from 61.26% in PNSC to 76.57% with PSC addition, reflecting enhanced carbonisation, while oxygen content correspondingly decreases, improving the biochar's energy quality.[65] The amounts of hydrogen and nitrogen are mostly constant, with slight increases, whereas sulphur is very low in PNSC but higher in literature samples. These factors could have an impact on emissions when the product is being used; however, it can be managed by blending other feeds.[65] Compared to SNS, which exhibits higher H/C (0.99) and O/C (0.71) ratios than BGS (0.92 and 0.39), the PNSC and PNSC + PSC (30 wt%) samples show lower H/C (0.62 and 0.56) and O/C (0.43 and 0.19) ratios, signifying greater aromaticity, carbonisation, and structural stability of the char.[66]

The bulk density of char improves slightly with PSC addition, enhancing handling and storage characteristics. pH remains alkaline across all modified samples, supporting their potential use in soil amendment applications. The ability of char to retain nutrients, immobilise heavy metals, and function as a soil amendment is improved by its alkaline pH. It increases microbial activity, balances off soil acidity, and enhances cation exchange capacity. Because alkaline biochar improves soil health and decreases pollutant mobility, it is useful in wastewater treatment, agriculture, and environmental cleanup.[67] The HHV of the PNSC and PNSC + PSC (30 wt%) was found to be 25.15 and 32.42 MJ kg^{-1}, confirming that the addition of plastics enhanced the HHV of chars. Similar reports were also reported on Jungle Cork Tree (JCT) and non-recyclable polyethylene terephthalate (NRPET) char.[40] The ash content was also found to be reduced by 3.77% with the addition of PSC, which indicates the suitability of char for energy material application.[40] Overall, additions enhance carbon content, reduce moisture and oxygen contents, and improve physical attributes without compromising basic chemical stability. Compared to BGS and SNS char, the modified chars offer superior elemental profiles and structural qualities, underscoring their potential for energy and environmental applications. The produced char, with a high carbon content, low moisture, and alkaline pH, is suitable for various energy and environmental applications, such as a solid fuel for combustion, a soil amendment to improve fertility, and an adsorbent

© 2025 The Author(s). Published by the Royal Society of Chemistry

Open Access Article. Published on 17 November 2025. Downloaded on 2/17/2026 10:41:37 PM.
This article is licensed under a Creative Commons Attribution-NonCommercial 3.0 Unported Licence.

Table 4 Physicochemical characterisation of char derived from PNS + PS blend at 550 °C

Analysis	PNSC	PNSC + PSC (30 wt%)	BGS[52]	SNS[52]
Moisture content (wt%)	0.22 ± 0.04	0.03 ± 0.03	—	—
Ash content (wt%)	8.25 ± 0.16	4.48 ± 0.14	—	—
C (%)	61.26 ± 0.12	76.57 ± 0.16	48.4	61.30
H (%)	3.18 ± 0.10	3.61 ± 0.10	04.0	4.70
N (%)	0.05 ± 0.01	0.05 ± 0.01	01.2	0.7
S (%)	—	—	00.5	1.0
O (%)	35.51 ± 0.01	19.77 ± 0.02	45.9	32.30
H/C	0.62	0.56	0.99	0.92
O/C	0.43	0.19	0.71	0.39
HHV (MJ kg^{-1})	25.15 ± 1.40	32.42 ± 1.60	—	26.40
Bulk density (kg m^{-3})	631.91 ± 11.85	689.03 ± 9.08	—	—
pH	8.19 ± 0.11	8.21 ± 0.14	—	—

for wastewater treatment, due to its enhanced stability, porosity, and nutrient-retention capacity.

3.10. FTIR analyses of char

FTIR analysis presented in Fig. 11 confirmed the functional group present in the char derived from PNSC, PNSC + PSC (30 wt%) and a blend using 5 wt% CuO. The plot between wavenumber and transmittance of char is present in Fig. 11. The spectra reveal significant differences in transmittance across the char derived from PNS, plastic blending, and catalysis blending. PNSC exhibits a moderate transmittance across the spectral range, with notable bands in the regions corresponding to C–H, C=O, and C–O functional groups. These indicate the presence of aliphatic hydrocarbons, carbonyl compounds, and oxygenated species, typical of biomass-derived pyrolysis char.[68] The introduction of PS at 30 wt% shows decreased absorption in the lower wavenumber region (500–1500 cm^{-1}), suggesting reduced oxygenated functionality and increased hydrocarbon content due to the polymeric nature of the plastic.[69] Peaks in the aromatic region (730–760 cm^{-1}) and at 3020 cm^{-1} (C–H stretching in aromatics) are more prominent, indicating the formation of aromatic hydrocarbons.[69]

The addition of CuO catalyst results in a marked increase in transmittance across the spectrum, particularly in the regions associated with polar functional groups (O–H and C=O), implying their effective decomposition or conversion.[70] The flatter profile with diminished peaks suggests that CuO promotes deoxygenation and cracking reactions, leading to a more refined, less polar pyrolysis oil and char composition. Overall, FTIR results demonstrate that co-pyrolysis with polystyrene enhances the aromatic hydrocarbon content. At the same time, CuO catalysis further improves oil quality by reducing oxygenated compounds, indicating synergistic effects of plastic blending and catalytic treatment on pyrolysis oil composition.

3.11. XRD analysis of char

The XRD plot of PNSC, PNSC + PSC (30 wt%) and PNSC + PSC (50 wt%) is presented in Fig. 12. The patterns span the 2θ range of approximately 5° to 60°, revealing distinct peaks that allow

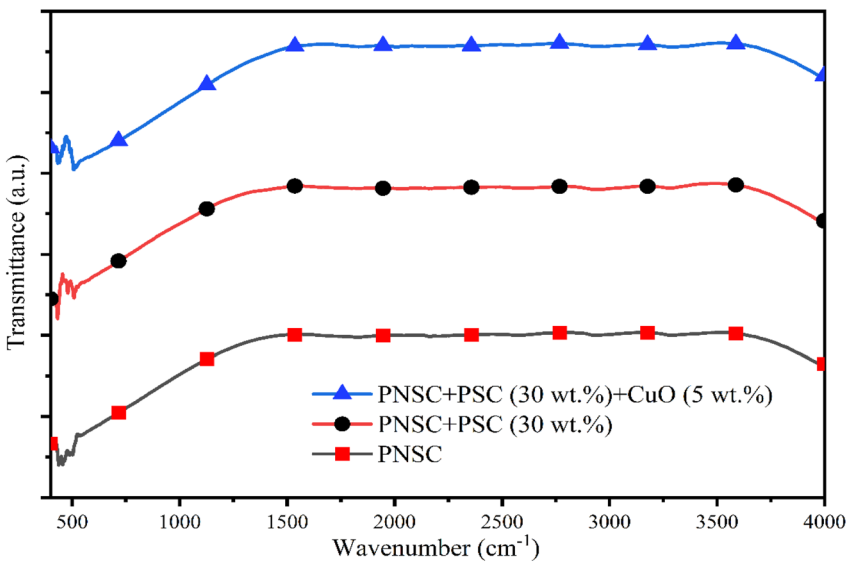

Fig. 11 Functional group analysis of char derived from different composites.

Open Access Article. Published on 17 November 2025. Downloaded on 2/17/2026 10:41:37 PM. This article is licensed under a Creative Commons Attribution-NonCommercial 3.0 Unported Licence.

for phase comparison and crystallinity assessment. The PNSC exhibits sharp and intense peaks at 23.13, 31.85, 45.57, and 56.31°, suggesting crystalline carbon structures, likely graphitic or turbostratic carbon. These peaks indicate well-ordered domains, with 31.85° often attributed to graphitic (002) planes, confirming high structural integrity in the carbon matrix.[71] Strong diffraction peaks observed at 31.85°, 45.57°, and 56.31° suggest the possible presence of fluorite, graphite, and chlorapatite phases. Additional lower-intensity peaks were attributed to calcite, bayerite, and hydrobiotite. Moreover, in the lower 2θ range, distinct peaks corresponding to apophyllite, pyrophyllite, and barite were also detected alongside graphite and fluorite.[71] In contrast, composite samples with PNS and PS (particularly at higher PS loadings) exhibit broader and less intense peaks, indicating reduced crystallinity resulting from polymer integration or structural disorder. Further, the XRD plot of PNSC + PSC (30 wt%) shows characteristic peaks at 22.65°, 31.85°, 43.60°, 45.83°, 50.73°, and 57.86°. These peaks imply the retention of partial crystalline order, possibly related to residual graphitic domains or mineral phases embedded within the polymer matrix. The peak at 45.83° is well-resolved in PNSC + PSC (30 wt%), whereas it diminishes in PNSC, indicating a loss of crystallinity with increasing PS content. A set of overlapping peaks in the 22°–23° region (22.55°, 22.65°, and 23.13°) suggests an amorphous-to-semi-crystalline transition region possibly influenced by disordered carbon or semi-crystalline polymer chains.[40] These shifts and broadenings are more evident in the blue curve, where peak merging and intensity reduction indicate a higher degree of structural disruption, likely due to increased PS content interfering with the regular packing of crystallites. Furthermore, PNSC + PSC 50 wt% exhibits peaks at 22.55°, 31.85°, 45.57°, and 56.31°, indicating the presence of residual crystalline phases, likely originating from amorphous carbon and degraded inorganic components. The reduced intensity and broadness suggest structural disorder, with partial retention of graphitic or mineral features disrupted by high polymer content. The prominent sharp peaks observed at 31.85° in PNSC + PSC 30 wt% and 50 wt% were attributed to the presence of chlorite and gibbsite. Alongside these dominant peaks, several medium-intensity peaks at 26.65°, 22.55°, 45.57°, 45.83°, 50.73°, 56.31°, and 57.86° indicated the presence of coquimbite, graphite, and hydrobiotite phases.[71] The reduction in peak intensities and increased baseline for the PNSC + PSC 50 wt% confirms the decline in overall crystallinity as polymer concentration increases, promoting amorphisation. This trend is consistent with the incorporation of non-crystalline or weakly crystalline polymeric materials into a carbon-rich matrix, diluting the diffraction contribution from well-ordered domains. Overall, the XRD pattern demonstrates that PNSC maintains the highest crystallinity, which gradually diminishes as PS loading increases in PNSC + PSC composites.[40] The composite with 30 wt% PS retains moderate crystallinity with clear diffraction peaks, while the 50 wt% sample exhibits significantly reduced order, highlighting the structural influence of polymer incorporation on the crystalline framework of the materials. This evolution in crystallinity reflects potential changes in thermal stability, conductivity, and mechanical behaviour due to matrix disruption and phase interaction. Waqas *et al.* (2018) produced the biochar at a dynamic temperature and reported similar results.[71]

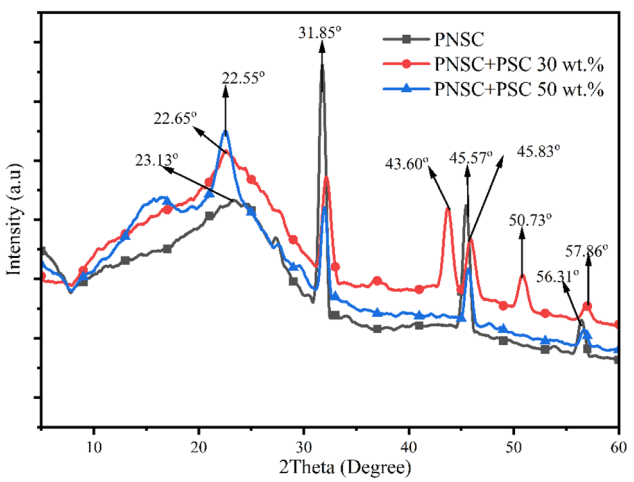

Fig. 12 XRD analysis of char obtained at thermal and co-pyrolysis at 30 and 50 wt%.

3.12. SEM analysis of char

SEM images of PNSC, PNSC + PSC (30 wt%) and PNSC + PSC (30 wt%) + CuO (5 wt%) are listed in Fig. 13a–c at 5 kX magnification. Fig. 13a shows he unmodified PNSC, exhibiting a denser and more aggregated structure with fewer visible pores and a smoother surface. The compact morphology observed here suggests a significantly lower surface area and limited exposure of active sites. Additionally, the surface structure of the char was found to be rough and irregular in terms of size and channel formation. Furthermore, PNSC + PSC (30 wt%) composite displays a fibrous morphology (Fig. 13b) but with slightly less defined pores and surface roughness compared to Fig. 13a. Although the addition of PSC contributes to the formation of a porous structure, it limits the overall textural development. Fig. 13c shows the PNSC + PSC(30 wt%) + CuO (5 wt%), revealing a highly porous and fibrous surface morphology with a well-developed network of interconnected channels. The presence of CuO appears to enhance the porosity and structural complexity, resulting in a rougher texture and a larger surface area. This suggests that CuO plays a synergistic role in enhancing the surface properties of the composite. This morphology suggests a better dispersion of the components and a more favourable structure for applications requiring high reactivity or adsorption capacity. Overall, the SEM analysis clearly demonstrates that the combined addition of PNS and CuO significantly improves the material's morphological properties, enhancing its surface area and porosity. These enhancements are particularly beneficial for various functional applications such as adsorption, catalysis, or electrochemical energy storage, where surface characteristics play a crucial role in performance.

© 2025 The Author(s). Published by the Royal Society of Chemistry

Open Access Article. Published on 17 November 2025. Downloaded on 2/17/2026 10:41:37 PM.
This article is licensed under a Creative Commons Attribution-NonCommercial 3.0 Unported Licence.

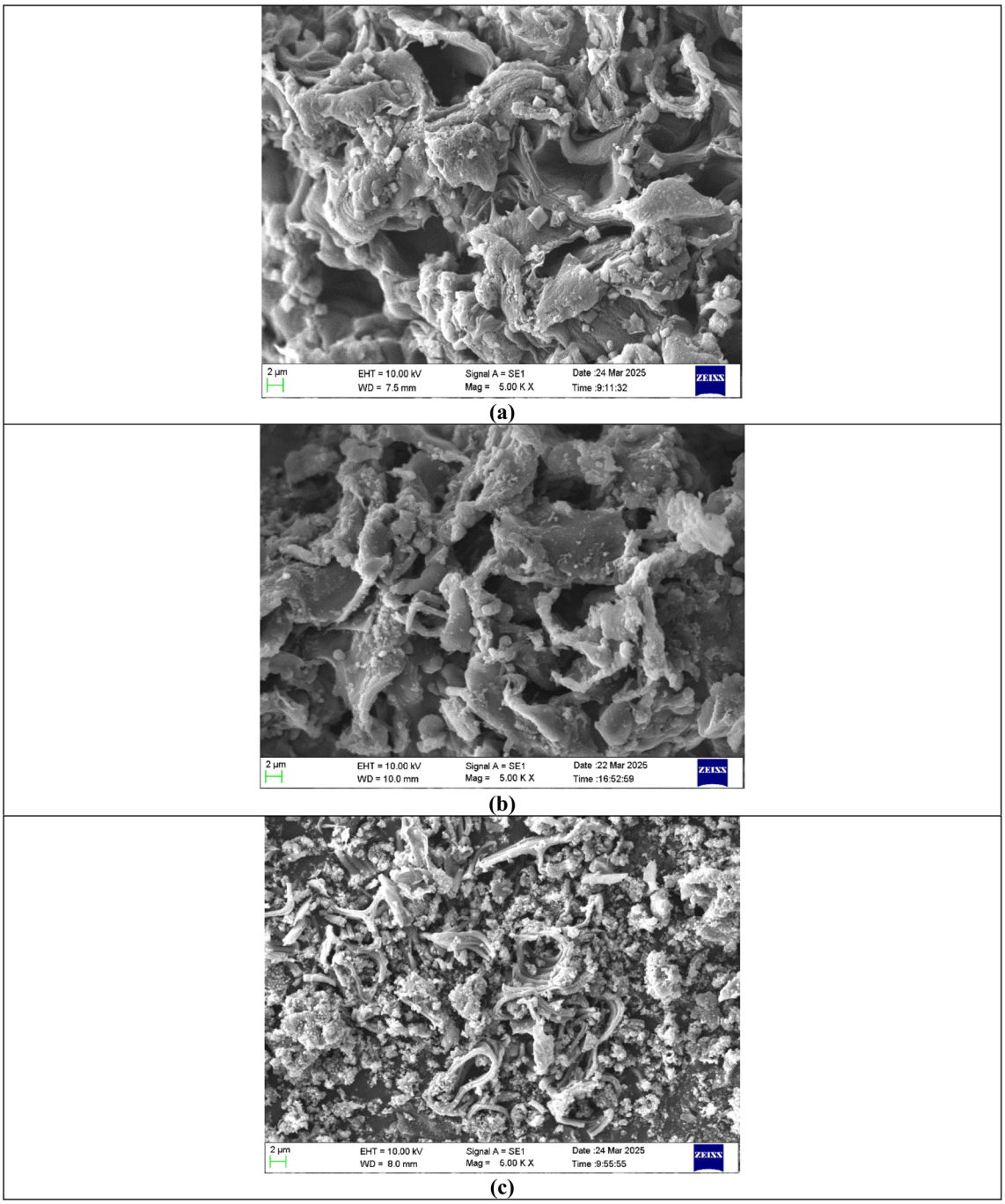

Fig. 13 Surface morphology analysis of char (a) PNSC, (b) PNSC + PSC (30 wt%) and (c) PNSC + PSC (30 wt%) + CuO (5 wt%).

4. Conclusions

This study successfully demonstrated the catalytic co-pyrolysis of pistachio nutshells (PNS) and polystyrene (PS) as an effective strategy for producing high-quality bio-oil and energy-rich char. The experimental optimisation revealed that a PS loading of 30 wt% at 550 °C produced the highest yield of liquid fuel, while CuO catalyst at 5 wt% further enhanced the quality of the pyrolysis oil by reducing oxygenated compounds and increasing its heating value. The synergy between biomass and plastic enhanced the hydrocarbon profile, improved fuel properties, and increased the stability of the bio-oil, making it a promising alternative to conventional fuels. Characterisation of the products confirmed enhanced physicochemical properties, including reduced acidity and viscosity of the oil, as well as higher carbon content and heating value in the char. The integration of waste biomass and plastic not only promotes sustainable waste management but also supports circular economy principles by converting low-value materials into energy-dense fuels. Furthermore, the study highlights the

Open Access Article. Published on 17 November 2025. Downloaded on 2/17/2026 10:41:37 PM.
This article is licensed under a Creative Commons Attribution-NonCommercial 3.0 Unported Licence.

significant role of metal oxide catalysts in tuning product distribution and improving fuel quality. Overall, this work provides a viable route for valorising agro-industrial and plastic waste through catalytic pyrolysis, contributing to renewable energy generation, resource efficiency, and environmental sustainability. Future research should focus on reactor scale-up and long-term stability of the products.

The current study demonstrates the potential of catalytic co-pyrolysis of PNS and PS using CuO catalyst, which has certain limitations. The experiments were performed in a semi-batch reactor under controlled laboratory conditions, which may not fully replicate the complex dynamics of large-scale continuous operations. Reactor heat and mass transfer uniformity, residence time distribution, and volatile condensation efficiency can vary significantly in industrial systems, potentially altering product yield and composition. Therefore, a systematic molecular study is required for better accuracy of the results. The catalyst was used in a physical mixing mode, which could result in non-uniform contact between the feed and catalyst particles, thus influencing the reaction kinetics and conversion efficiency. Another limitation lies in the lack of long-term catalyst stability and recyclability assessments; sintering, deactivation, or carbon deposition on CuO during repeated use could influence its efficiency. Furthermore, although the produced pyrolysis oil exhibits improved heating value and lower oxygen content, it still contains residual oxygenated and acidic compounds, indicating the need for further post-processing such as hydrotreatment or advanced catalytic upgrading to refine its quality and meet commercial fuel specifications. The compositional variability of waste biomass and plastics also poses a challenge to process reproducibility and product uniformity. Future research should focus on scaling up the reactor design, optimising heat transfer and vapour recovery systems, and performing continuous flow trials to assess operational stability. Exploring alternative and bimetallic catalysts (*e.g.*, Cu–Ni, Zn–Fe) or supported catalysts could further enhance selectivity toward hydrocarbon-rich fractions and minimise secondary cracking. Furthermore, in-depth kinetic and thermodynamic modelling would help predict reaction behaviour and energy efficiency at scale. Long-term studies assessing catalyst regeneration, life-cycle emissions, and techno-economic feasibility are essential to transition this process toward industrial viability. Also, integrating product upgrading steps with co-pyrolysis in a single process chain could enhance overall efficiency and product quality. Investigations into co-feeding diverse biomass–plastic mixtures and their effect on product properties will also broaden the application potential. Overall, this study provides a solid foundation for waste-to-fuel valorisation. Addressing these limitations will be vital for achieving sustainable, large-scale implementation and aligning with circular economy and carbon neutrality goals.

Conflicts of interest

The authors announce that they have no known competing financial interests or personal relationships that could have appeared to influence the work presented in this paper.

Author contributions

Rohit Dutta, Harsh Desai, and Tanushka Florence Panicker: sample collection, data interpretation and experimentation, Ranjeet Kumar Mishra: conceptualisation, data curation, methodology, investigation, visualisation, writing – original draft, and supervision, Sampath Chinnam, Srinivas Kini Manjeshwar and Pradeep Kumar: investigation, visualisation, software, editing draft, and supervision.

Data availability

The datasets generated during and/or analysed during the current study are available from the corresponding author upon reasonable request.

Supplementary information is available. See DOI: **https://doi.org/10.1039/d5ra06092c**.

Acknowledgements

The author would like to thank Biomass Bioenergy and Bioproducts Lab (3B Lab) and Department of Chemical Engineering, Manipal Institute of Technology, Manipal, Ramaiah Institute of Technology, Bangalore and Indian Institute of Technology Varanasi, India, for providing all the facilities.

References

1 S. Yi, K. R. Abbasi, K. Hussain, A. Albaker and R. Alvarado, *Gondwana Res.*, 2023, **117**, 41–55.
2 D. Kour, K. L. Rana, N. Yadav, A. N. Yadav, A. A. Rastegari, C. Singh, P. Negi, K. Singh and A. K. Saxena, *Prospects of Renewable Bioprocessing in Future Energy Systems*, 2019, pp. 1–50.
3 C. C. Seah, C. H. Tan, N. A. Arifin, R. S. R. M. Hafriz, A. Salmiaton, S. Nomanbhay and A. H. Shamsuddin, *Results Eng.*, 2023, **17**, 100989.
4 N. Tripathi, C. D. Hills, R. S. Singh and C. J. Atkinson, *npj Clim. Atmos. Sci.*, 2019, **2**, 35.
5 R. Thahir, M. Irwan, A. Alwathan and R. Ramli, *Results Eng.*, 2021, **11**, 100231.
6 C. J. Rhodes, *Sci. Prog.*, 2019, **102**, 218–248.
7 T. Thiounn and R. C. Smith, *J. Polym. Sci.*, 2020, **58**, 1347–1364.
8 M.-N. Kaydouh and N. El Hassan, *Results Eng.*, 2022, **16**, 100771.
9 B. B. Uzoejinwa, X. He, S. Wang, A. E.-F. Abomohra, Y. Hu and Q. Wang, *Energy Convers. Manage.*, 2018, **163**, 468–492.
10 R. Hossain, M. T. Islam, A. Ghose and V. Sahajwalla, *J. Cleaner Prod.*, 2022, **368**, 133127.
11 S. Ashoor, T. U. Khang, Y. H. Lee, J. S. Hyung, S. Y. Choi, S. E. Lim, J. Lee, S. J. Park and J.-G. Na, *Bioresour. Bioprocess.*, 2023, **10**, 34.
12 C. Ma, J. Geng, D. Zhang and X. Ning, *J. Energy Inst.*, 2020, **93**, 303–311.

© 2025 The Author(s). Published by the Royal Society of Chemistry

Open Access Article. Published on 17 November 2025. Downloaded on 2/17/2026 10:41:37 PM. This article is licensed under a Creative Commons Attribution-NonCommercial 3.0 Unported Licence.

13 Y. Buyang, S. Suprapto, R. E. Nugraha, H. Holilah, H. Bahruji, R. Hantoro, A. A. Jalil, T. P. Oetami and D. Prasetyoko, *J. Anal. Appl. Pyrolysis*, 2023, **169**, 105852.
14 F. Chireshe, F.-X. Collard and J. F. Görgens, *J. Cleaner Prod.*, 2020, **260**, 120987.
15 F. Abnisa and W. M. A. W. Daud, *Energy Convers. Manage.*, 2014, **87**, 71–85.
16 M. Carrier, A. Loppinet-Serani, D. Denux, J.-M. Lasnier, F. Ham-Pichavant, F. Cansell and C. Aymonier, *Biomass Bioenergy*, 2011, **35**, 298–307.
17 R. M. Dineshkumar, K. M. S. Begum and A. Ramanathan, *Mater. Today: Proc.*, 2021, **46**, 9837–9843.
18 A. Almendros, M. Martín-Lara, A. Ronda, A. Pérez, G. Blázquez and M. Calero, *Bioresour. Technol.*, 2015, **196**, 406–412.
19 R. K. Mishra and R. Vinu, *J. Anal. Appl. Pyrolysis*, 2024, **179**, 106514.
20 S. Mehanathan, P. Madhu, C. S. Dhanalakshmi and R. Vijayakumar, *J. Energy Inst.*, 2025, **118**, 101905.
21 M. Alam, A. Bhavanam, A. Jana, J. k. S. Viroja and N. R. Peela, *Renew. Energy*, 2020, **149**, 1133–1145.
22 F. G. Fonseca, A. Funke, A. Niebel, A. P. S. Dias and N. Dahmen, *J. Anal. Appl. Pyrolysis*, 2019, **139**, 73–86.
23 P. Doshi, G. Srivastava, G. Pathak and M. Dikshit, *Waste Manage.*, 2014, **34**, 1836–1846.
24 T. Kan, V. Strezov and T. J. Evans, *Renewable Sustainable Energy Rev.*, 2016, **57**, 1126–1140.
25 A. Nawaz, R. K. Mishra, S. Sabbarwal and P. Kumar, *Bioresour. Technol. Rep.*, 2021, 100858.
26 S. Mooninta, S. Poompradub and P. Prasassarakich, *J. Polym. Environ.*, 2020, **28**, 3116–3128.
27 T. Y. Fahmy, Y. Fahmy, F. Mobarak, M. El-Sakhawy and R. E. Abou-Zeid, *Environ. Dev. Sustain.*, 2020, **22**, 17–32.
28 I. M. Maafa, *Polymers*, 2021, **13**, 225.
29 M. Schweiger, T. Lang, D. Touraud, E. Müller and W. Kunz, *RSC Sustainability*, 2025, **3**, 4514–4532.
30 K. Mensah, H. Mahmoud, M. Fujii and H. Shokry, *Key Eng. Mater.*, 2021, **897**, 103–108.
31 R. K. Mishra and K. Mohanty, *Mater. Sci. Energy Technol.*, 2020, **3**, 526–535.
32 R. K. Mishra and K. Mohanty, *J. Renewable Sustainable Energy*, 2018, **10**, 013102.
33 R. K. Mishra and K. Mohanty, *Bioresour. Technol.*, 2018, **251**, 63–74.
34 V. Chintala, S. Kumar, J. K. Pandey, A. K. Sharma and S. Kumar, *Energy Convers. Manage.*, 2017, **153**, 482–492.
35 R. K. Mishra and K. Mohanty, *Renew. Energy*, 2019, **141**, 549–558.
36 D. S. Achilias, I. Kanellopoulou, P. Megalokonomos, E. Antonakou and A. A. Lappas, *Macromol. Mater. Eng.*, 2007, **292**, 923–934.
37 K. Polat and E. A. Bursalı, *J. Mater. Cycles Waste Manage.*, 2019, 1–7.
38 N. Rambhatla, T. F. Panicker, R. K. Mishra, S. K. Manjeshwar and A. Sharma, *Results Eng.*, 2025, **25**, 103679.
39 M. Hashemi, K. T. Q. Nguyen, D. J. Robert, G. K. Zhang, T. Hosseinnejad and D. Marney, *J. Anal. Appl. Pyrolysis*, 2026, **193**, 107360.
40 R. K. Mishra, *RSC Sustain.*, 2025, **3**, 1774–1787.
41 G. Greco, M. Videgain, C. Di Stasi, E. Pires and J. J. Manyà, *J. Anal. Appl. Pyrolysis*, 2021, **159**, 105337.
42 D. V. Suriapparao, D. A. Kumar and R. Vinu, *Sustain. Energy Technol. Assessments*, 2022, **49**, 101781.
43 A. S. Al-Fatesh, N. Y. AL-Garadi, A. I. Osman, F. S. Al-Mubaddel, A. A. Ibrahim, W. U. Khan, Y. M. Alanazi, M. M. Alrashed and O. Y. Alothman, *Fuel*, 2023, **344**, 128107.
44 A. Imran, E. A. Bramer, K. Seshan and G. Brem, 2018.
45 R. K. Mishra, R. Saini, D. J. P. Kumar, R. Sankannavar, P. Binnal, N. Dwivedi and P. Kumar, *J. Energy Inst.*, 2023, **111**, 101366.
46 S. Shao, W. Wang, X. Yang, Z. Ye, J. Sun and X. Li, *Fuel*, 2023, **353**, 129028.
47 A. Dewangan, D. Pradhan and R. K. Singh, *Fuel*, 2016, **185**, 508–516.
48 R. Kumar Mishra and K. Mohanty, *Carbon Resour. Convers.*, 2020, **3**, 145–155.
49 B. B. Uzoejinwa, X. He, S. Wang, A. El-Fatah Abomohra, Y. Hu and Q. Wang, *Energy Convers. Manage.*, 2018, **163**, 468–492.
50 E. J. Paz-García, S. P. Paredes-Carrera, S. O. Flores-Valle, I. S. Rodríguez-Clavel, J. C. Sánchez-Ochoa and R. M. Pérez-Gutiérrez, *Appl. Sci.*, 2019, **9**, 5525.
51 N. Podrojková, J. Patera, R. Popescu, J. Škoviera, R. Oriňaková and A. Oriňak, *ChemistrySelect*, 2021, **6**, 4256–4264.
52 M. D. Ibrahim, Y. A. Abakr, S. Gan and S. Thangalazhy-Gopakumar, *Environ. Technol.*, 2024, **45**, 1870–1883.
53 A. H. Fombu, A. Ochonogor, A. E. Ochonogor and O. E. Olayide, in *Proceedings of the sustainable, clean and emerging energy technologies conference, UNESCO international centre for biotechnology*, University of Nigeria, Nsukka, 2024, pp. 206–215.
54 J. B. Omwoyo, R. K. Kimilu and J. M. Onyari, *Chem. Eng. Commun.*, 2023, **210**, 1086–1096.
55 A. M. de Morais Araújo, R. de Oliveira Lima, A. D. Gondim, J. Diniz, L. Di Souza and A. S. de Araujo, *Renew. Energy*, 2017, **101**, 900–906.
56 Q. An, Y. Liu, X. Cao, P. Yang, L. Cheng, M. S. Ghazani, M. J. Suota and X. Bi, *J. Anal. Appl. Pyrolysis*, 2024, **182**, 106683.
57 K. P. Shadangi and K. Mohanty, *Fuel*, 2014, **117**, 372–380.
58 J. Joseph, C. Baker, S. Mukkamala, S. H. Beis, M. C. Wheeler, W. J. DeSisto, B. L. Jensen and B. G. Frederick, *Energy Fuels*, 2010, **24**, 5153–5162.
59 N. S. Tessarolo, R. V. S. Silva, G. Vanini, A. Casilli, V. L. Ximenes, F. L. Mendes, A. de Rezende Pinho, W. Romão, E. V. R. de Castro, C. R. Kaiser and D. A. Azevedo, *J. Anal. Appl. Pyrolysis*, 2016, **117**, 257–267.
60 K. G. Kalogiannis, S. D. Stefanidis, C. M. Michailof, A. A. Lappas and E. Sjöholm, *J. Anal. Appl. Pyrolysis*, 2015, **115**, 410–418.
61 P. A. Horne and P. T. Williams, *Fuel*, 1996, **75**, 1051–1059.

Open Access Article. Published on 17 November 2025. Downloaded on 2/17/2026 10:41:37 PM.
This article is licensed under a Creative Commons Attribution-NonCommercial 3.0 Unported Licence.

62 H. R. Ong, M. R. Khan, M. Chowdhury, A. Yousuf and C. K. Cheng, *Fuel*, 2014, **120**, 195–201.
63 C. Chen, S. Qiu, H. Ling, J. Zhao, D. Fan and J. Zhu, *Ind. Crops Prod.*, 2023, **199**, 116756.
64 S. Joseph, *Biochar for Environmental Management: Science, Technology and Implementation*, Routledge, 2015.
65 B. Sajjadi, W.-Y. Chen and N. O. Egiebor, *Rev. Chem. Eng.*, 2019, **35**, 735–776.
66 C. Nzediegwu, M. A. Naeth and S. X. Chang, *J. Anal. Appl. Pyrolysis*, 2021, **156**, 105174.
67 X. Gao, J. Yang, W. Liu, X. Li, W. Zhang and A. Wang, *Environ. Res.*, 2023, **233**, 116084.
68 A. Ray, A. Banerjee and A. Dubey, *International Journal of Agriculture, Environment and Biotechnology*, 2020, **13**, 423–430.
69 R. R. Nair, M. M. Mondal and D. Weichgrebe, *Biomass Convers. Biorefin.*, 2022, **12**, 4729–4743.
70 R. K. Mishra and K. Mohanty, *Biochar*, 2021, **3**, 641–656.
71 M. Waqas, A. Aburiazaiza, R. Miandad, M. Rehan, M. Barakat and A. Nizami, *J. Cleaner Prod.*, 2018, **188**, 477–488.

© 2025 The Author(s). Published by the Royal Society of Chemistry